ONCOIMMUNOLOGY
2018, VOL. 7, NO. 6, e1433518 (16 pages)
https://doi.org/10.1080/2162402X.2018.1433518

Taylor & Francis
Taylor & Francis Group

ORIGINAL RESEARCH

OPEN ACCESS Check for updates

Choice of costimulatory domains and of cytokines determines CAR T-cell activity in neuroblastoma

Concetta Quintarelli[a,b,*], Domenico Orlando[a], Iolanda Boffa[a], Marika Guercio[a], Vinicia Assunta Polito[a], Andrea Petretto[c], Chiara Lavarello[c], Matilde Sinibaldi[a], Gerrit Weber[a], Francesca Del Bufalo[a], Ezio Giorda[d], Marco Scarsella[d], Stefania Petrini[d], Daria Pagliara[a], Franco Locatelli[a,e,*], Biagio De Angelis[a,§], and Ignazio Caruana[a,§]

[a]Department of Pediatric Hematology and Oncology, IRCCS Ospedale Pediatrico Bambino Gesù, Rome, Italy; [b]Department of "Medicina Clinica e Chirurgia", University of Naples Federico II, Naples, Italy; [c]Core Facilities-Proteomics Laboratory, Istituto Giannina Gaslini, Genoa, Italy; [d]Core Facilities, IRCCS Ospedale Pediatrico Bambino Gesù, Rome Italy; [e]Department of Pediatrics, University of Pavia, Pavia, Italy

ABSTRACT

Chimeric antigen receptor (CAR) T-cell therapy has been shown to be dramatically effective in the treatment of B-cell malignancies. However, there are still substantial obstacles to overcome, before similar responses can be achieved in patients with solid tumors. We evaluated both *in vitro* and in a preclinical murine model the efficacy of different 2nd and 3rd generation CAR constructs targeting GD2, a disialganglioside expressed on the surface of neuroblastoma (NB) tumor cells. In order to address potential safety concerns regarding clinical application, an inducible safety switch, namely inducible Caspase-9 (iC9), was also included in the vector constructs. Our data indicate that a 3rd generation CAR incorporating CD28.4-1BB costimulatory domains is associated with improved anti-tumor efficacy as compared with a CAR incorporating the combination of CD28.OX40 domains. We demonstrate that the choice of 4-1BB signaling results into significant amelioration of several CAR T-cell characteristics, including: 1) T-cell exhaustion, 2) basal T-cell activation, 3) *in vivo* tumor control and 4) T-cell persistence. The fine-tuning of T-cell culture conditions obtained using IL7 and IL15 was found to be synergic with the CAR.GD2 design in increasing the anti-tumor activity of CAR T cells. We also demonstrate that activation of the suicide gene iC9, included in our construct without significantly impairing neither CAR expression nor anti-tumor activity, leads to a prompt induction of apoptosis of GD2.CAR T cells. Altogether, these findings are instrumental in optimizing the function of CAR T-cell products to be employed in the treatment of children with NB.

ARTICLE HISTORY
Received 17 November 2017
Revised 20 January 2018
Accepted 22 January 2018

KEYWORDS
Chimeric antigen receptor (CAR); CAR.GD2 design; CD28.4-1BB costimulatory domains; Neuroblastoma; T-cell exhaustion; solid tumors

Introduction

Use of T cells genetically modified to express a chimeric antigen receptor (CAR) is a new promising approach of adoptive T-cell immunotherapy for cancer, combining antigen specificity of a monoclonal antibody (mAb) with effector function, active biodistribution and long-term persistence of T cells.[1-4] Despite the relevant clinical benefit of CAR-T cells in the treatment of $CD19^+$ acute lymphoblastic leukemia,[5] targeting of solid tumors has thus far shown limited efficacy, due to multiple factors, including a suppressive tumor microenvironment,[6,7] variables in CAR engineering,[8] the definition of optimal targets, antigen heterogeneity and antigen-loss variants(9). In the context of neuroblastoma (NB), mAbs recognizing the cell-surface disial-ganglioside GD2 have been developed, and clinical studies documented a benefit in terms of maintenance/consolidation of a state of remission in patients with high-risk NB treated with these mAbs.[10-12]

After more than 10 years from the first clinical trial using CAR T-cell technology, there is substantial agreement on the importance of adequate expansion and persistence of CAR-T cells *in vivo* for achieving consistent and durable anti-tumor activity, especially in the setting of solid tumors.[13-16] A phase I clinical trial with a 1st generation CAR.GD2 in patients with NB showed a transient clinical response associated with only limited persistence of CAR-T cells.[17,18] Importantly, an improved efficacy, as well as a longer persistence of CAR-T cells, were demonstrated with genetically modified, EBV-specific T cells activated by the engagement of their native T-cell receptor, indicating the importance of additional co-stimulatory domains for clinical efficacy.

In view of all these findings, understanding how the CAR structure influences the *in vivo* behavior of adoptively transferred T cells is extremely relevant. Recently, the central role of

CONTACT Franco Locatelli, MD, PhD franco.locatelli@opbg.net Piazza Sant'Onofrio, 400165 Rome, Italy; Dr. Concetta Quintarelli, PhD concetta.quintarelli@opbg.net Viale di San Paolo 15, 00145, Rome, taly.

Supplemental data for this article can be accessed on the publisher's website.

*These Authors are both Corresponding Authors.

§These Authors contributed equally as Last Author.

© 2018 Concetta Quintarelli, Domenico Orlando, Iolanda Boffa, Marika Guercio, Vinicia Assunta Polito, Andrea Petretto, Chiara Lavarello, Matilde Sinibaldi, Gerrit Weber, Francesca Del Bufalo, Ezio Giorda, Marco Scarsella, Stefania Petrini, Daria Pagliara, Franco Locatelli, Biagio De Angelis and Ignazio Caruana. Published with license by Taylor & Francis Group, LLC
This is an Open Access article distributed under the terms of the Creative Commons Attribution-NonCommercial-NoDerivatives License (http://creativecommons.org/licenses/by-nc-nd/4.0/), which permits non-commercial re-use, distribution, and reproduction in any medium, provided the original work is properly cited, and is not altered, transformed, or built upon in any way.

CAR design in chronic T-cell activation and exhaustion has been demonstrated: CD28 costimulation was shown to augment, whereas 4-1BB costimulation to reduce exhaustion induced by persistent CAR signaling.[8] Moreover, while the superiority of 2nd and 3rd generation over 1st generation CAR T cells has been clearly shown in both preclinical and clinical studies,[5,19–21] the optimal combination of costimulatory domains for 3rd generation CAR-T cells remains to be defined and should be evaluated case-by-case in order to fine-tune immunotherapy approaches.

With the scope of identifying the best experimental conditions able to ameliorate the biological properties of CAR T cells in humans and, thus, to optimize clinical results of CAR T-cell therapy in children with NB, we designed and tested different 2nd and 3rd generation CAR.GD2 constructs. Although pre-clinical data in NB have not yet demonstrated a clear advantage of 3rd generation CAR constructs ($_{III}$CAR.GD2) compared to 2nd generation ($_{II}$CAR.GD2),[22] several studies suggest a benefit of a stronger T-cell activation, such as that offered by 3rd generation constructs for CAR T-cells.[23,24] Therefore, in our study, we mainly focused our investigations on $_{III}$CAR.GD2 incorporating an endodomain that transmits two costimulatory signals, one from the immunoglobulin co-receptor superfamily (CD28) and the other either from one of the tumor necrosis factor receptor family members OX40 or from 4-1BB.[8,25,26] Moreover, since the use of CAR-T cells has been reported to induce in some patients life-threatening or even fatal side effects, such as cytokine release syndrome[27-29] or neurological toxicities,[30-32] we decided to investigate whether the incorporation in the construct of a suicide gene, namely the inducible caspase 9 (iC9),[33] may improve the safety, without impairing the efficacy of CAR.GD2 T cells. Overall, the data we obtained indicate that, in the context of CAR.GD2 expressing the 14. G2a-derived single chain, both the costimulatory machinery and *in vitro* exposure to pleiotropic cytokines are crucial for improving the persistence and ultimately the antitumor efficacy of the approach and that iC9 can be added to the CAR constructs without altering the anti-tumor efficacy of the cells.

Results

The choice of costimulatory domain influences the proliferation rate of $_{III}$CAR.GD2 T cells upon extended in vitro *culture*

Our initial results showed no significant differences in terms of cytotoxic and anti-tumor activities between $_{II}$CAR.GD2 (including as costimulatory molecule either CD28, or OX40 or 4–1BB) and $_{III}$CAR.GD2 T cells, as assessed in both *in vitro* (data not shown) and *in vivo* experiments (supplementary Fig. 1A). However, improved persistence of $_{III}$CAR.GD2 T cells was observed in our *in vivo* mouse model (Supplementary Fig. 1B). Therefore, in view of these findings and of previously published results,[7,22,34] we continued our study focusing on $_{III}$CAR.GD2 to proceed with the further implementation of the approach. We optimized the construct encompassing the single-chain variable fragment (scFv) derived from 14.G2a mAb, in frame with CD28, and either OX40 or 4–1BB as a second costimulatory domain; the CD3-zeta chain (ζ) was also included in the construct as T-cell signaling domain.

No difference in transduction efficiency of primary T cells was observed between the $_{III}$CAR.GD2 constructs (namely CARGD2.28.4–1BBζ or CARGD2.28.OX40ζ) (Fig. 1A–B). Although lower than that of un-transduced T-cells (NT), the expansion rate of these two type of $_{III}$CAR.GD2 T cells was superimposable during the first two weeks of culture. Thereafter, CAR.GD2.28.4–1BBζ T cells and NT displayed a similar expansion rate, whereas CAR.GD2.28.OX40ζ reached a *plateau* (Fig. 1C). For characterization of both basal and induced proliferation, CFSE analyses were performed on day+15 of culture. CARGD2.28.OX40ζ T cells exhibited a significantly higher level of basal proliferation than CARGD2.28.4–1BBζ T cells (Fig. 1D), although this difference was subsequently lost either upon activation by the anti-idiotype 1A7 (Fig. 1E) or exposure to IL2 (data not shown).

The costimulatory domain in $_{III}$CAR.GD2 significantly modulates in vivo, *but not* in vitro *activity of CAR T cells expanded with IL2*

To compare the cytolytic activity of $_{III}$CAR.GD2 T cells including either of the two different costimulatory signalling domains, a standard 6-hr ^{51}Cr release assay was performed. Fig. 2A and 2B show that $_{III}$CAR.GD2 T cells, expressing either CD28.4–1BB or CD28.OX40 selectively kills with the same efficiency GD2^{+} NB tumor cell lines (SHSY5Y and IMR-32), but not the SHSY5Y GD2(negative) subclone (Fig. 2C) or the leukemia cell line K562 (data not shown). Nevertheless, when $_{III}$CAR.GD2 T cells with the two different costimulatory signalling domains were tested in a xenograft NSG mouse model, we observed that only CARGD2.28.4–1BBζ T cells mediated sustained anti-tumor effects *in vivo* (Fig. 2D–F). In detail, a SHSY5Y/FF-Luc. GFP tumor model was established and tumor growth after infusion of T cells at day 0 was analyzed by measuring the bioluminescence signal. As shown in Fig. 2D–F, in the control group treated with NT cells, tumor bioluminescence progressively increased over time. Similarly, most mice that had received CARGD2.28.OX40ζ T cells experienced a rapid tumor growth. By contrast, in the CARGD2.28.4–1BBζ T cell-treated mice, efficient long-term tumor control was observed, this translating into a significantly better 60-day disease-free survival (DFS) (76.9%, compared to 17.1% for mice treated with CARGD2.28.OX40ζ and 0% for mice given NT cells) ($p = 0.013$ and $p = 0.002$, respectively) (Fig. 2F).

Identification of a peculiar basal phospho-proteomic profile of $_{III}$CAR.GD2

To understand the influence of the costimulatory domains on both resting (basal) and activated $_{III}$CAR.GD2 T cells, we employed a high throughput phospho-proteomic approach to identify qualitative and quantitative differences between phospho-sites in both CD4^{+} and CD8^{+} CAR T-cell populations. Utilizing the MaxQuant software and label-free quantification, we identified 20,246 phosphorylation sites associated with

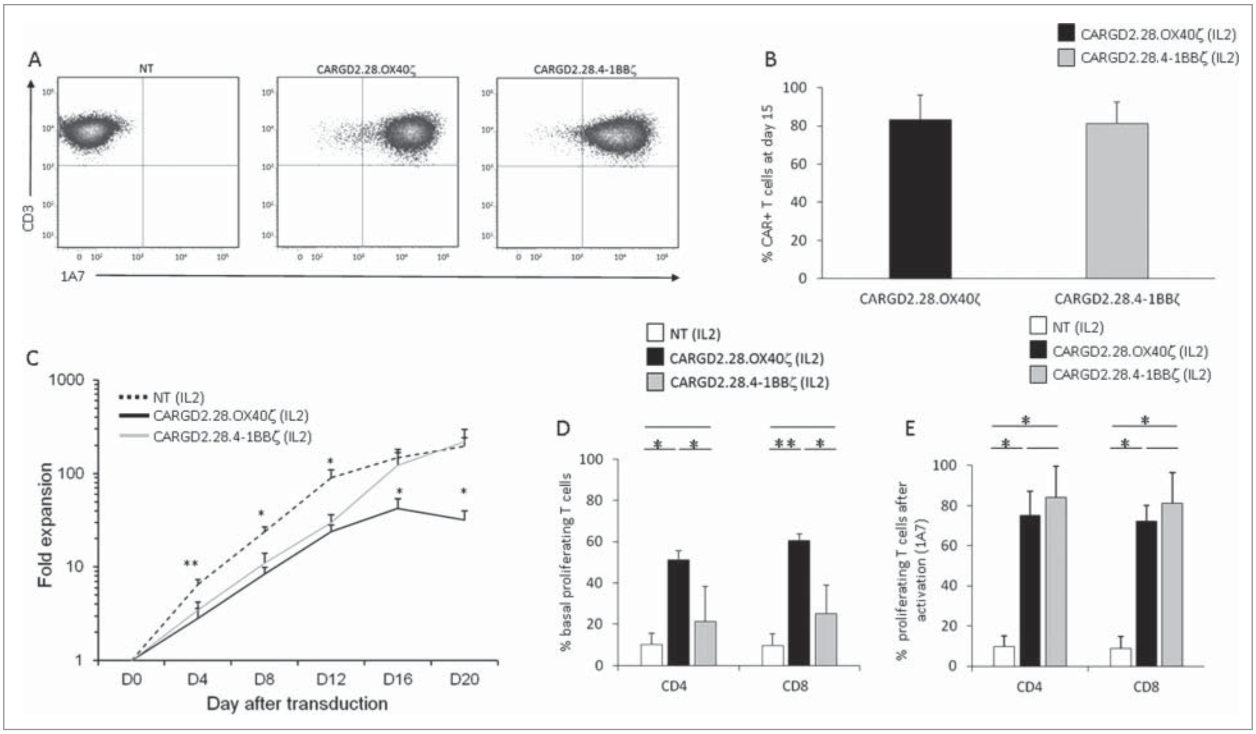

Figure 1. Characterization of CAR.GD2 T cells. (A) Representative flow-cytometry analysis of NT (left panel), CARGD2.28.OX40ζ (middle panel) or CARGD2.28.4–1BBζ (right panel) T cells derived from a healthy donor (HD) 15 days after transduction and culture in a medium containing IL2. CAR expression was detected using a specific anti-idiotype antibody (1A7). (B) $CD3^{+}$ CAR.GD2 T cells present in the CAR T-cell production 15 days after transduction in the presence of IL2. Data from 7 HDs are expressed as average $\pm$ standard deviation (SD). (C) Fold expansion of NT (black dashed line), CARGD2.28.OX40ζ (black line) and CARGD2.28.4–1BBζ (gray line) T cells in the presence of IL2. Data from 7 HDs are expressed as average $\pm$ SD. (D-E) Percentage of proliferating (evaluated by CFSE) NT (white bar), CARGD2.28.OX40ζ (black bar) and CARGD2.28.4–1BBζ (gray bar) T cells monitored for 7 days in the absence of stimulation (D) or activated by specific stimulation with the 1A7 antibody (E). Data from 3 HDs are expressed as average $\pm$ SD. $^{**}p < 0.01$ and $^{*}p < 0.05$; t-test.

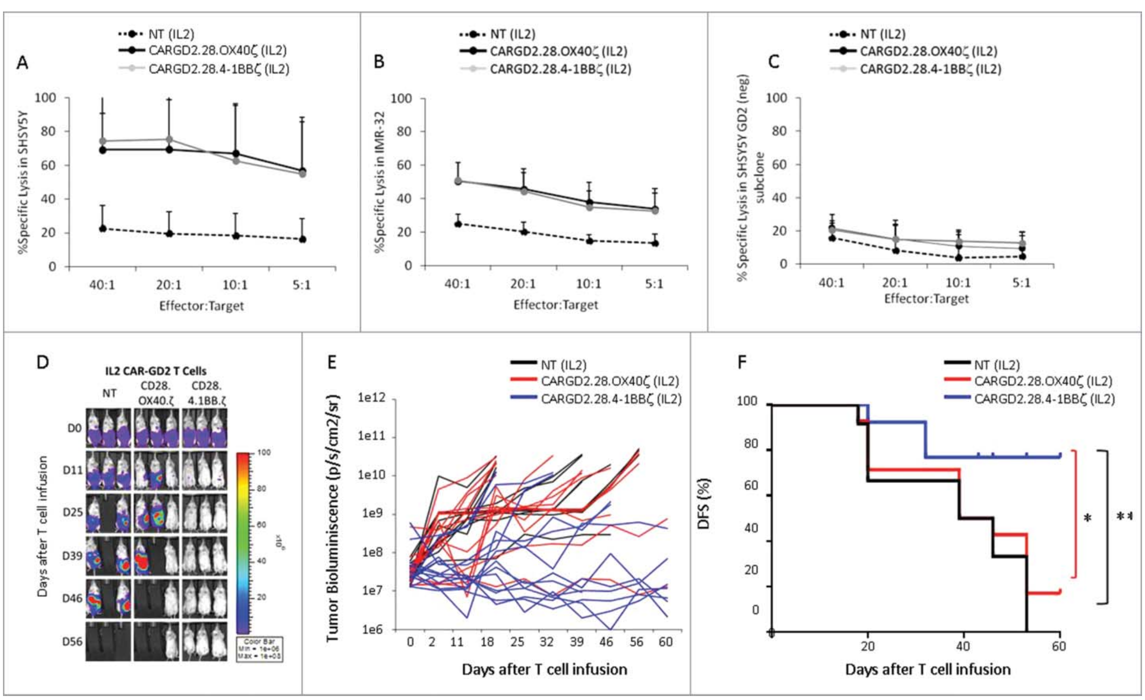

Figure 2. 28.4–1BB and 28.OX40 costimulatory domains show comparable *in vitro* results, whereas only CARGD2.28.4–1BBζ T cells exert long-lasting *in vivo* antitumor response. (A-C) *In vitro* ^{51}Cr release assay evaluating cytolytic activity of NT (black dotted line), CARGD2.28-OX40ζ (black line) and CARGD2.28.4–1BBζ T cells (gray line), on $GD2^{+}$ NB SHSY5Y tumor cell line (A), $GD2^{+}$ IMR-32 cell line (B), and SHSY5Y GD2(neg) subclone (C). Assays were performed 15 days after initial activation and expansion in the presence of IL2. Data from 4 HDs are expressed as average $\pm$ SD. (D-E) *In vivo* bioluminescence imaging of NSG mice bearing i.p. SHSY5Y-FF-Luc.GFP cells and treated with NT, CARGD2.28.OX40ζ or CARGD2.28.4–1BBζ T cells (D) bioluminescence imaging of 3 representative mice per group; (E) bioluminescence of each single mouse treated with NT (black line, 12 mice), CARGD2.28.OX40ζ (red line, 14 mice) and CARGD2.28.4–1BBζ T cells (blue line, 14 mice). (F) 60-day probability of disease-free survival (DFS) of NSG mice bearing i.p. SHSY5Y-FF-Luc.GFP cells after adoptive i.p. transfer of NT (black line, 12 mice), CARGD2.28.OX40ζ (red line, 14 mice) and CARGD2.28.4–1BBζ T cells (blue line, 14 mice). $^{**}p < 0.01$ and $^{*}p < 0.05$.

4,533 proteins, achieving a high phospho-proteome coverage. The phospho-site analysis showed a clearly different distribution between CARGD2.28.OX40ζ and CARGD2.28.4–1BBζ (Fig. 3A) T cells, with a significantly higher number of phosphorylated sites in both CD4$^+$ and CD8$^+$ CARGD2.28.OX40ζ than in CARGD2.28.4–1BBζ T cells (Anova Test with a FDR < 0.01 and S0 > 0.1). Moreover, the *Venn* diagram showed a common core of 4,637 sites for $_{III}$CAR.GD2 CD4$^+$ (Fig. 3B) and one of 4,542 sites for $_{III}$CAR.GD2 CD8$^+$ (Fig. 3C) T cells, respectively. This overlap of sites matched with a set of common biological processes shared between the two kinds of $_{III}$CAR.GD2 T cells. Noteworthy, the number of phospho-sites was higher in both basal and activated CD4$^+$ and CD8$^+$ CARGD2.28.OX40ζ than in CARGD2.28.4–1BBζ T cells. In

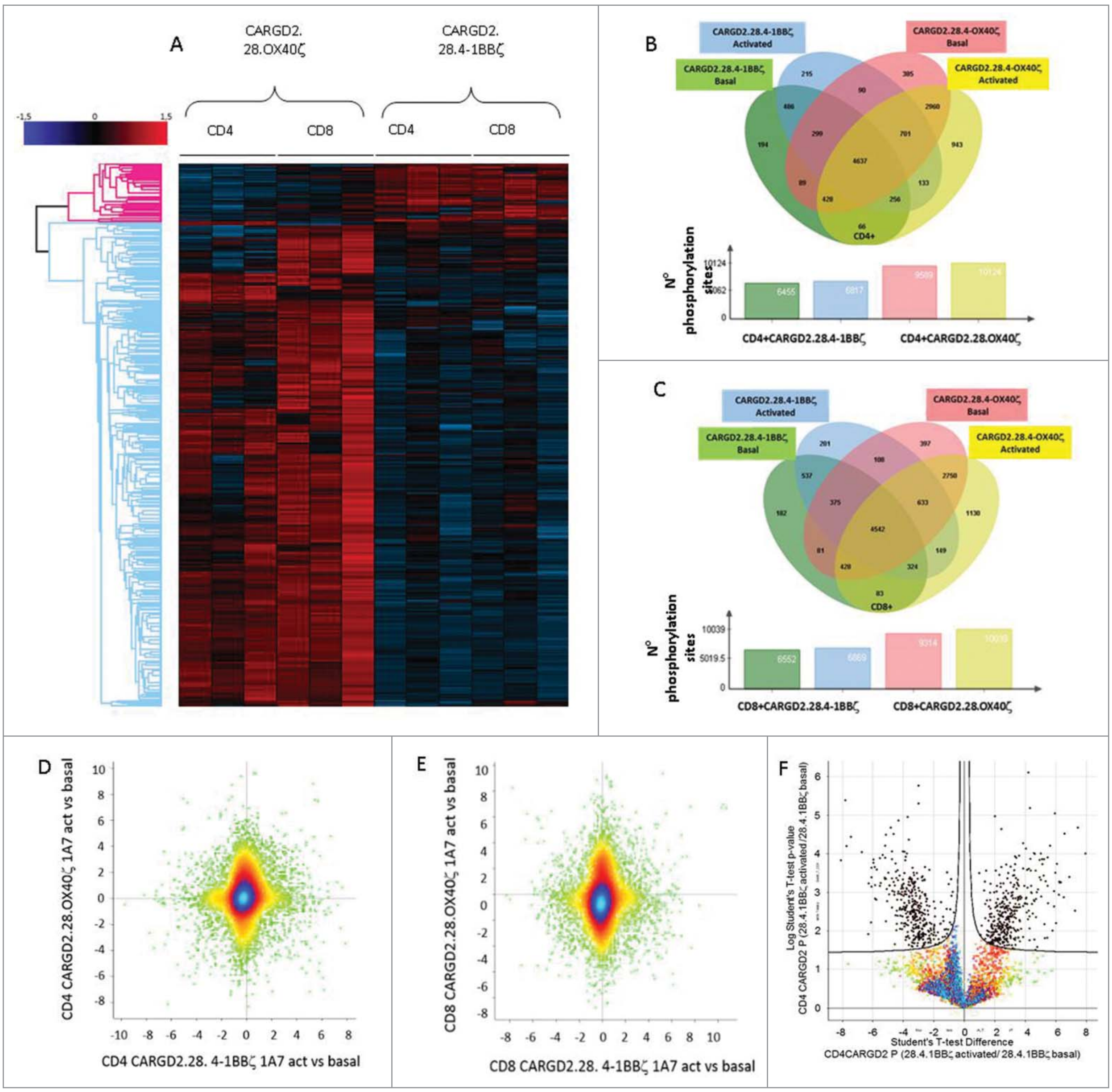

Figure 3. Phospho-proteomic profile of $_{III}$CAR.GD2 T cells and membrane distribution of CAR.GD2 molecules. (A) Anova graphical representation of the differential phospho-proteome pattern in CD4$^+$ and CD8$^+$ subsets of $_{III}$CAR.GD2 resting T cells; 3 HDs. Heat map showing average log2 values of phosphosite intensities after normalization. (B-C) *Venn diagram* of phosphorylation sites detected in CD4$^+$ (B) and CD8$^+$ (C) subsets of $_{III}$CAR.GD2 T cells at basal conditions or after 1A7-activated T cells; 3 HDs. Numbers represent the distinct phosphorylation sites in the respective overlapping and non-overlapping areas; the histograms below show the total number of phosphorylation sites involved in all the analyzed groups. (D-E) *Profile plot* showing the comparison of quantitative MS phosphoproteomes with distinct profiles for CD4$^+$ (D) and CD8$^+$ (E) $_{III}$CAR.GD2 T cells in terms of distance from the density center. The normalized intensities are expressed as log2. (F-I) *Volcano plots* represent differentially expressed phosphosites in CD4$^+$ (F-G) and CD8$^+$ (H-I) $_{III}$CAR.GD2 T cells, respectively; 3 HDs. The plots represent the differences between activation profiles in CARGD2.28.4–1BBζ (F-H) and CARGD2.28.OX40ζ (G-I) T cells after 1A7-specific activation. Black dots represent phosphosites that display both large magnitude fold-changes (x-axis, to the right there are proteins up-regulated after treatment), as well as high statistical significance (-log10 of p-value, y-axis). Colored dots represent proteins whose fold-change is < 2 (log2 = 1) or p>0.05 and they are close in the two dataset. (J) Confocal images of NT, $_{II}$CAR.GD2 (28ζ, OX40ζ and 4–1BBζ) and $_{III}$CAR.GD2 (28.OX40ζ and 28.4–1BBζ) T cells. CAR.GD2 molecules are stained in green, plasma membranes in red and nuclei in blue. Merge Figs. are displayed in the third row, while 3D Z-surface reconstructions in the bottom row. (K) Representation of differential sizes distribution of CAR isosurfaces, quantified by IMARIS software, in $_{II}$CAR.GD2 and $_{III}$CAR.GD2 T cells. At least 100 T cells were evaluated in each experiment. On the top right, a magnification of a cluster bigger than 10 μ^3. ****p < 0,0001, ***p < 0.001, **p < 0.01 and *p < 0.05; t-test. (L) Representative picture of the dynamic time-lapse co-culture studying the interaction between T cells and tumor. GFP$^+$/GD2$^+$ NB tumor cell lines (green) were co-cultured with $_{III}$CAR.GD2 and analyzed by confocal live imaging. The immunological synapses were detected by actin polymerization (red).

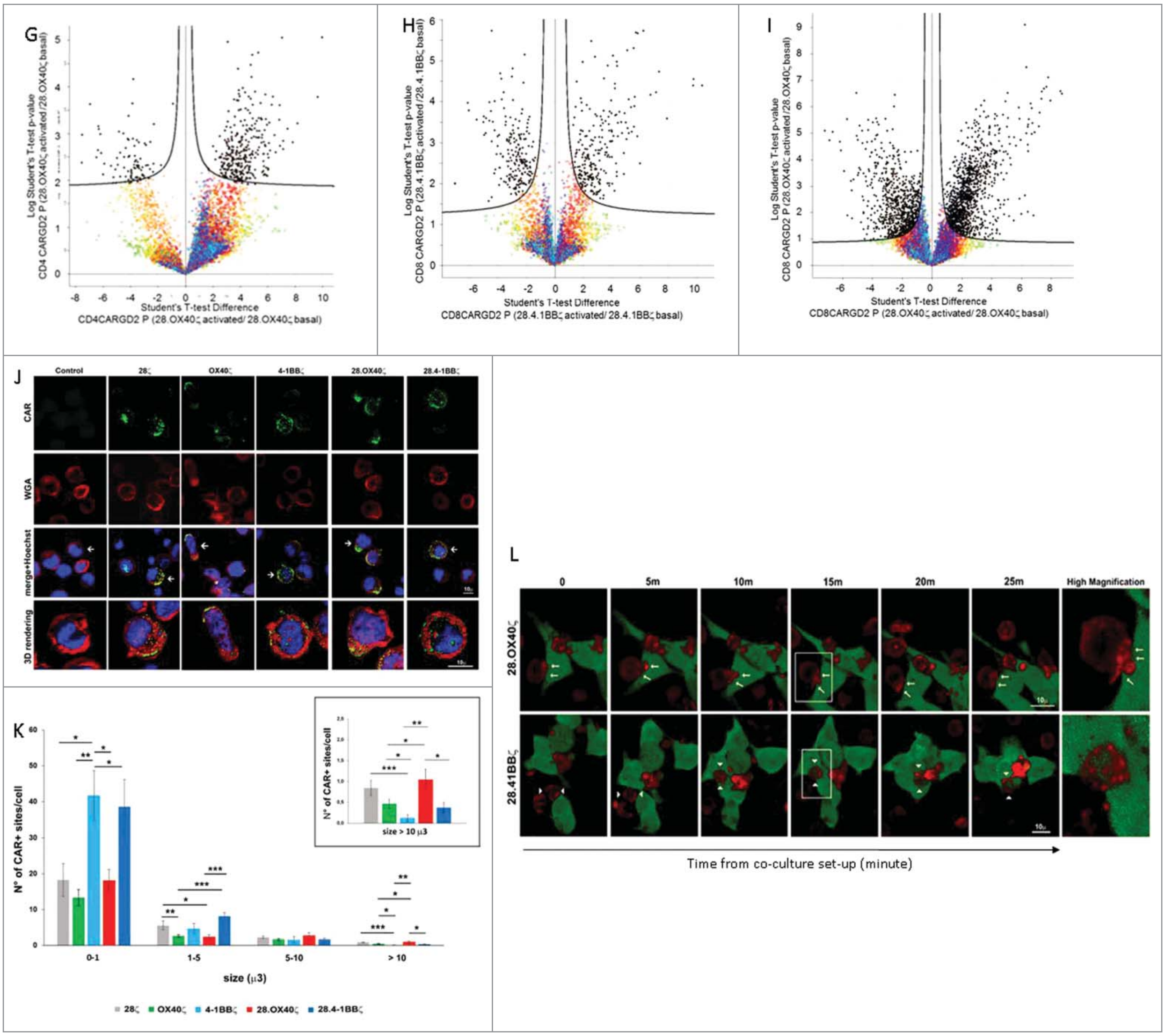

Figure 3. (continued).

order to directly compare the two ${}_{III}$CAR.GD2 T-cell populations, masking the background effect and taking into account the intensity/abundance of phosphorylation sites, we mapped the mass spectrometry (MS) profiles on a two-dimensional scatter plot (Fig. 3D–E), where the observed pronounced stretching of the colored points highlights the differences related to the higher number of phospho-sites observed in CARGD2.28.OX40ζ as compared to CARGD2.28.4–1BBζ T cells. The Volcano plot confirmed the differential and increased phospho-proteome pattern in activated CD4^{+} (Fig. 3F–G) and CD8^{+} CARGD2.28.OX40ζ (Fig. 3H–I) with respect to CARGD2.28.4–1BBζ T cells. Subsequently, in order to highlight the different pathways regulated by 28.OX40 and 28.4–1BB, we performed a network analysis by Cytoscape on the proteins associated with the identified phosphorylation sites, showing the involvement of several key networks of cell activation, proliferation, apoptosis and senescence for CD8^{+} ${}_{III}$CAR.GD2 T-cell populations (Supplementary Fig. 2) and CD4^{+} ${}_{III}$CAR.GD2 T-cell populations (Supplementary Fig. 3). Moreover, the analysis of the absolute numbers of phosphorylated sites after GD2-specific activation in both CD4^{+} and CD8^{+} ${}_{III}$CAR.GD2 T cells in various pathways underlines the difference of the two constructs. This difference correlates with the biological behavior and activity observed in both in vitro and in vivo studies. In Supplementary Table 1, we report an excerpt of pathways demonstrating these differences, including cytokine production (Supplementary Fig. 5) and proliferation rate (Fig. 1C and 4D–E). Moreover, we validated the results of the phosphoproteomic profile by WB, showing a higher phosphorylation level of CD3 zeta (pY83) in CARGD2.28.OX40ζ T cells than in CARGD2.28.4–1BBζ T (Supplementary Fig. 4). This finding strongly correlates with the higher number of protein sites phosphorylated in the TCR signaling pathway seen in CARGD2.28.OX40ζ T cells respect to CARGD2.28.4–1BBζ T cells.

Different costimulatory domains influence CAR.GD2 clustering on T cells

In order to understand the mechanisms involved in the basal activation observed in CARGD2.28.OX40ζ T cells, we investigated the cell membrane distribution of CAR molecules in

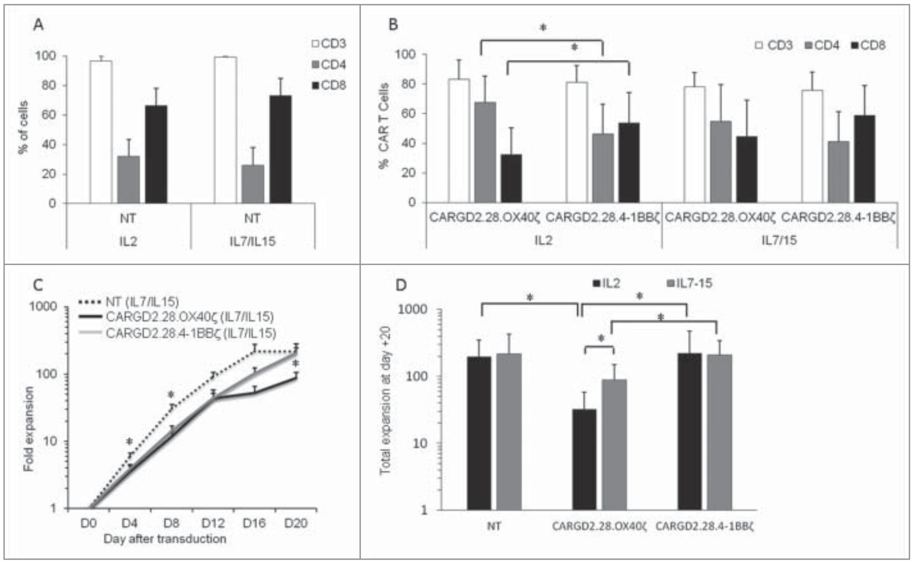

Figure 4. Composition and expansion profile of $_{III}$CAR.GD2 T cells. (A) Flow-cytometry analysis of the percentage of CD3$^+$ (white bar), CD4$^+$ (gray bar) and CD8$^+$ (black bar) of NT expanded for 15 days in presence of IL2 or IL7/IL15. Data from 7 HDs are expressed as average ± SD. (B) Flow-cytometry analysis of the percentage of CD3$^+$ (white bar), CD4$^+$ (gray bar) and CD8$^+$ (black bar) of $_{III}$CAR.GD2 T cells expanded for 15 days in presence of IL2 or IL7/IL15. Data from 7 HDs are expressed as average ± SD. (C) Fold expansion of NT (black dashed line), CARGD2.28.OX40ζ (black line) and CARGD2.28.4–1BBζ (gray line) T cells in the presence of IL7/IL15. Data from 7 HDs are expressed as average ± SD. $^*p < 0.05$; t-test. (D) Data from 7 HDs are expressed as average ± SD of total fold expansion at day+20 of *in vitro* culture of NT or $_{III}$CAR.GD2 T cells in presence of IL2 (black bars) or IL7/IL15 (gray bars). $^*p < 0.05$; t-test.

$_{II}$CAR.GD2 and $_{III}$CAR.GD2 sharing the same scFv. Using confocal microscopy, we observed a clear difference between the two $_{III}$CAR.GD2 constructs (Fig. 3J), with CARGD2.28.OX40ζ showing strong oligomerization and polarization on the cell surface, similar to that observed in T cells transduced with a 2nd generation CAR incorporating either CD28 or OX40 as costimulatory domain. By contrast, CARGD2.28.4–1BBζ appears more uniformly distributed across the T-cell surface, similarly to $_{II}$CAR.GD2 incorporating 4–1BB only. Quantification of 3D reconstructions of CAR clusters, performed by IMARIS software, allowed detection of significant differences in the CAR domains/cell volume ratio between distribution groups

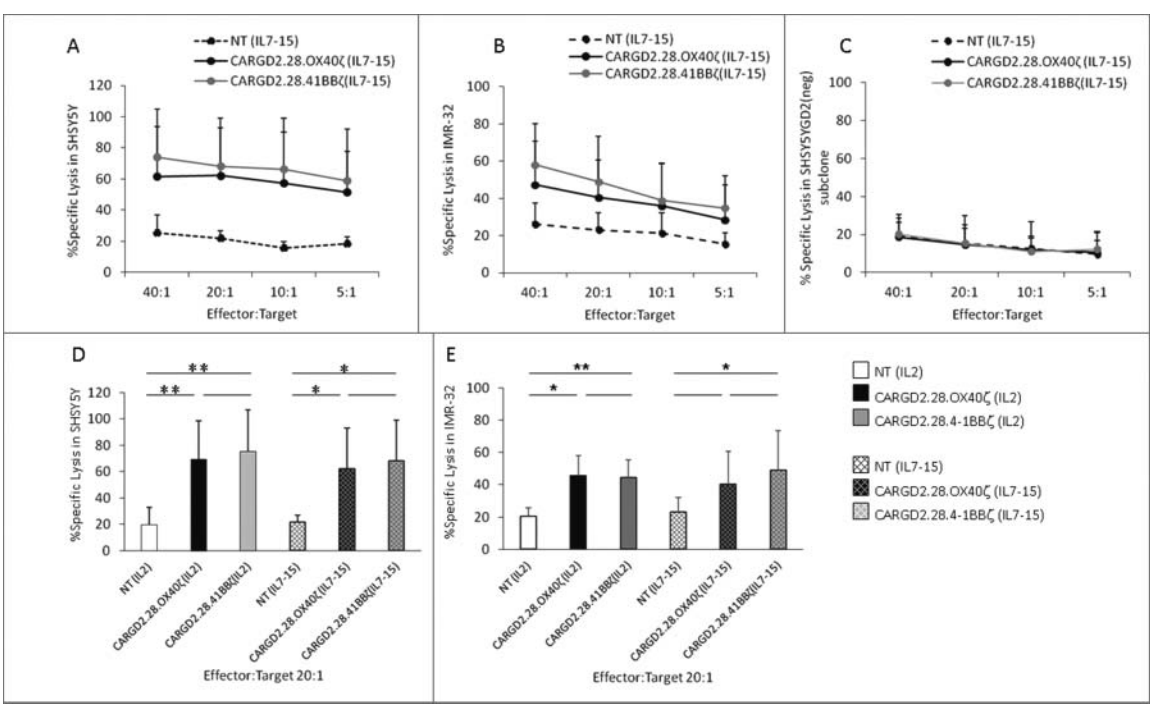

Figure 5. $_{III}$CAR.GD2 T cells grown in IL7/IL15 show comparable cytotoxic activities in short term *in vitro* assays. *In vitro* ^{51}Cr release assay evaluating cytolytic activity of NT (black dotted line), CARGD2.28.OX40ζ (black line) and CARGD2.28.4–1BBζ T cells (gray line), on GD2$^+$ NB SHSY5Y tumor cell line (A), GD2$^+$ IMR-32 cell line (B), and SHSY5Y GD2(neg) subclone (C). Assay performed 15 days after initial activation and expansion in the presence of IL7/IL15. Data from 4 HDs are expressed as average ± SD. (D-E) *In vitro* ^{51}Cr release assay evaluating cytolytic activity at the E:T ratio of 20:1, of NT (white bar), CARGD2.28.OX40ζ (black bar) and CARGD2.28.4–1BBζ T cells (gray bar), in presence of IL2 (plain colour bars) or IL7/IL15 (tiled colour bars). GD2$^+$ NB SHSY5Y tumor cell line (D) or GD2$^+$ IMR-32 cell line (E) were used as targets; data from 4 HDs are expressed as average ± SD.

(Fig. 3K). Furthermore, the dimensional classification of CAR clusters evidenced a higher number of small "clumps" in CARGD2.28.4–1BBζ than in CARGD2.28.OX40ζ T cells (Fig. 3K); conversely, larger CAR clusters, with sizes greater than 10 μ^3, were mainly detected in CARGD2.28.OX40ζ T cells (Fig. 3K).

Based on these results, we evaluated whether the CAR distribution may play a role in tumor engagement and killing. We performed a time-lapse live analysis of effector:target (E:T) co-culture by detection of polymerized F-actin through SiR-actin probe (Fig. 3L). CARGD2.28.OX40ζ T cells showed immune-synapse formation only in one or a few sites on T cells, while GD2.28.4–1BBζ T cells showed several bonding sites inducing almost complete wrapping of tumor cells (Fig. 3L, *arrows*).

Cytokines used in culture conditions influence in vitro *characteristics of $_{III}$CAR.GD2 T cells*

We and other authors recently reported that the combination of IL7/IL15 provides the best culture conditions for expansion of CAR-T cells.[35-39] Thus, we investigated the influence of these cytokines on CAR T-cell functions, in the context of different conditions of costimulation. While the percentage of CD4$^+$ or CD8$^+$ NT cells was not influenced by the presence of the cytokines (Fig. 4A), after 15 days of *in vitro* expansion with IL2, we observed a significantly higher percentage of CD4$^+$ in the CARGD2.28.OX40ζ, than in the CARGD2.28.4–1BBζ T-cell populations (Fig. 4B). The percentage of CD4$^+$ CARGD2.28.OX40ζ T cells was reduced when the culture medium contained IL7/IL15, reaching a value comparable to that of CARGD2.28.4–1BBζ T cells grown in the presence of either IL2 or IL7/IL15 (Fig. 4B). Moreover, IL7/IL15 had a significant impact on $_{III}$CAR.GD2 T-cell expansion. At day+20 of culture, CARGD2.28.OX40ζ T cells, when grown with IL7/IL15, showed a higher expansion as compared to those grown in the presence of IL2. By contrast, no differences were observed for both NT and CARGD2.28.41BBζ T cells (Fig. 4C–D). Cytokine culture conditions did not influence the *in vitro* specific cytolytic activity of $_{III}$CAR.GD2 T cells against GD2$^+$ NB cells, when tested in both standard cytotoxicity assay (Fig. 5A–E) and long-term co-culture (Fig. 6A–B). Tumor recognition remains specific also in the presence of IL7/IL15, as shown by the lack of killing of GD2-negative NB cells (Fig. 6C). Nevertheless, the activity of $_{III}$CAR.GD2 T cells at low E:T ratios showed a significant improvement of *in vitro* tumor control using IL7/IL15 as compared to IL2 in CARGD2.28.4–1BBζ T cells (Fig. 6D). We also demonstrated that neither the co-stimulatory domains, nor the cytokine used for *in vitro* expansion affected the T-cell receptor repertoire of CAR-T cells, which maintained polyclonality (data not shown).

The ability of the suicide gene iC9 to eliminate iC9/CAR T cells upon exposure to the dimerizing agent AP1903 was clearly demonstrated for both construct $_{III}$CAR.GD2; it was not influenced by the co-stimulatory domains and the cytokines used during the production process (Fig. 6E).

Cytokine culture conditions do not influence the in vitro *cytokine production of $_{III}$CAR.GD2 T cells upon tumor encounter*

We profiled cytokine production by 15-day expanded $_{III}$CAR.GD2 T cells upon antigen-specific stimulation through the

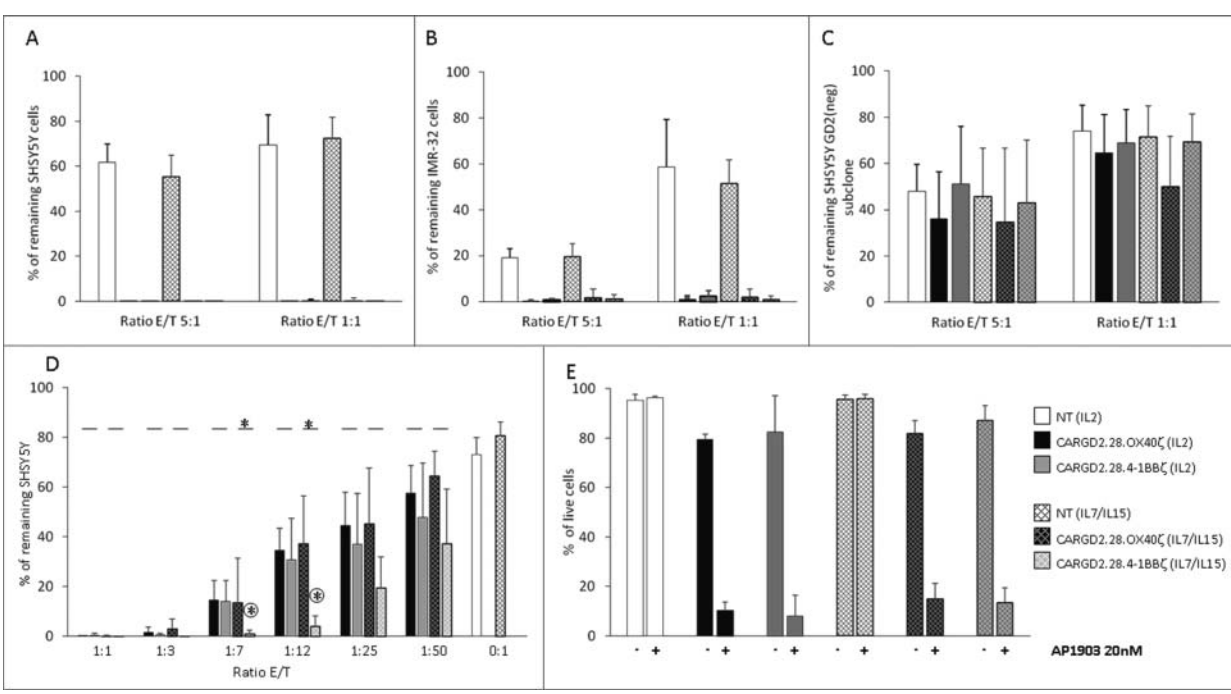

Figure 6. Long-term *in vitro* assay to evaluate functional activities of $_{III}$CAR.GD2 T cells. (A-B) Tumor cell growth after 7 days in co-culture experiments with CAR T cells at the E:T ratio 5:1 or 1:1 with NT (white bar), CARGD2.28.OX40ζ (black bar) and CARGD2.28.4–1BBζ T cells (gray bar), grown in IL2 (plain colour bars) or IL7/IL15 (tiled colour bars). GD2$^+$ NB SHSY5Y tumor cell line (A), GD2$^+$ IMR-32 cell line (B) or SHSY5Y GD2(neg) subclone (C) were used as targets. Data from 6 HDs are expressed as average $\pm$ SD in A-C; *p-value = <0.05. (D) Tumor cell growth after 7 days of co-culture at low E:T ratios with NT (white bar), CARGD2.28.OX40ζ (black bar) and CARGD2.28.4–1BBζ T cells (gray bar), grown in IL2 (plain colour bars) or IL7/IL15 (tiled colour bars). The GD2$^+$ NB SHSY5Y tumor cell line was used as target. Data from 4 HDs are expressed as average $\pm$ SD for (D); *p $<$ 0.05. (E) Annexin-V/7AAD staining of NT (white bar), CARGD2.28.OX40ζ (black bar) and CARGD2.28.4–1BBζ T cells (gray bar) grown in IL2 (plain colour bars) or IL7/IL15 (tiled colour bars) and exposed to 20 nM AP1903 for 24 h. Data from 4 HDs are expressed as average $\pm$ SD.

simultaneous analysis of multiple cytokines on supernatant collected after 24 hours of co-culture at an E:T ratio of 1:1, using SHSY5Y GD2$^+$ NB cells. The presence of the $_{III}$CAR.GD2 molecules in T cells did not significantly influence the basal production of Macrophage Inflammatory Protein-3A (MIP3 A), as well as that of IL23 and its up- and downstream factors IL17E[40] and IL17F,[41] both well-known biomarkers associated with inflammatory conditions. These results were comparable to those observed in NT (data not shown). Upon specific antigen stimulation, $_{III}$CAR.GD2 T cells produced high levels of Th2 cytokines, such as IL5 and IL13, with no significant difference according to the two constructs or the cytokines used for culturing CAR T cells (data not shown). Moreover, specific antigen stimulation was associated with high levels of Th1 cytokine production, with CARGD2.28.OX40ζ (IL2) T cells secreting a significantly lower amount of IFNγ (10.6 ng/ml ±4.3 ng/ml) and higher amount of IL2 (8.5 ng/ml ± 5.4 ng/ml) and TNFα (7.09 ng/ml ± 1.35 ng/ml) as compared to CARGD2.28.4–1BBζ T cells (28.2 ng/ml ± 15.7 ng/ml, $p = 0.016$; 1.8 ng/ml ± 1.0 ng/ml, $p = 0.031$; 4.6 ng/ml ± 1.5 ng/ml, $p = 0.562$; respectively) regardless of the presence in the culture of either IL2 or IL7/IL15 (Supplementary Fig. 5 A-C). Antigen-specific stimulation of CARGD2.28.OX40ζ T cells was also associated with higher secretion of pro-inflammatory cytokines, such as IL9, IL21 and IL6 (Supplementary Fig. 5D-F), with no significant difference related to the choice of the culture cytokines. All the other cytokines tested, including Th17-associated ones, were significantly increased, as compared to controls, upon antigen stimulation, to the same extent in the two constructs of $_{III}$CAR.GD2 T cells, irrespective of culture conditions. All these data were confirmed using a different GD2$^+$ NB cell line, IMR-32, as target (data not shown).

To evaluate the effects of long-term *in vitro* expansion, we evaluated the cytokine profile of 30-day expanded $_{III}$CAR.GD2 T cells in the supernatant collected after 24 hours of co-culture, at 1:1 ratio, with SHSY5Y GD2$^+$ NB cells. In these co-cultures, we observed that CARGD2.28.OX40ζ (IL2) T cells produced cytokines typical of a more exhausted profile, with lower amount of IL2 (0.3 ng/ml ± 0.2 ng/ml) and significantly lower level of IFNγ (2.3 ng/ml ± 0.4 ng/ml), compared to CARGD2.28.4–1BBζ T cells (2.5 ng/ml ±1.6 ng/ml, $p = 0.5$ ns; 7.3 ng/ml ±1.2 ng/ml, $p = 0.02$), respectively. These differences were particularly pronounced in T cells cultured in the presence of IL2 (Supplementary Fig. 6 A-B).

Co-stimulation domains and cytokine exposure influence T-cell phenotype and exhaustion profile in $_{III}$CAR.GD2 T cells

To evaluate the influence of specific costimulatory domains and cytokines employed in the culture medium on $_{III}$CAR.GD2 T-cells, we characterized both CD4$^+$ and CD8$^+$ CAR T cells for the expression of memory markers. In both CD4$^+$ and CD8$^+$ subsets, the majority of expanded T cells generated after CD3/CD28 stimulation and cultured with either IL2 or IL7/IL15 had an Effector Memory (EfM) phenotype (Fig. 7A–B). Moreover, in CARGD2.28.4–1BBζ T cells expanded in the presence of IL7/IL15, we observed a significantly higher percentage of Effector Terminal (EfT) than in T cells grown in IL2 (Fig. 7A). The pattern of co-inhibitory receptors (i.e. PD-1, LAG3 and TIM3) simultaneously expressed by CAR T cells was also evaluated in order to define their exhaustion status. We observed that, when $_{III}$CAR.GD2 T cells are cultured with IL2, the expression of

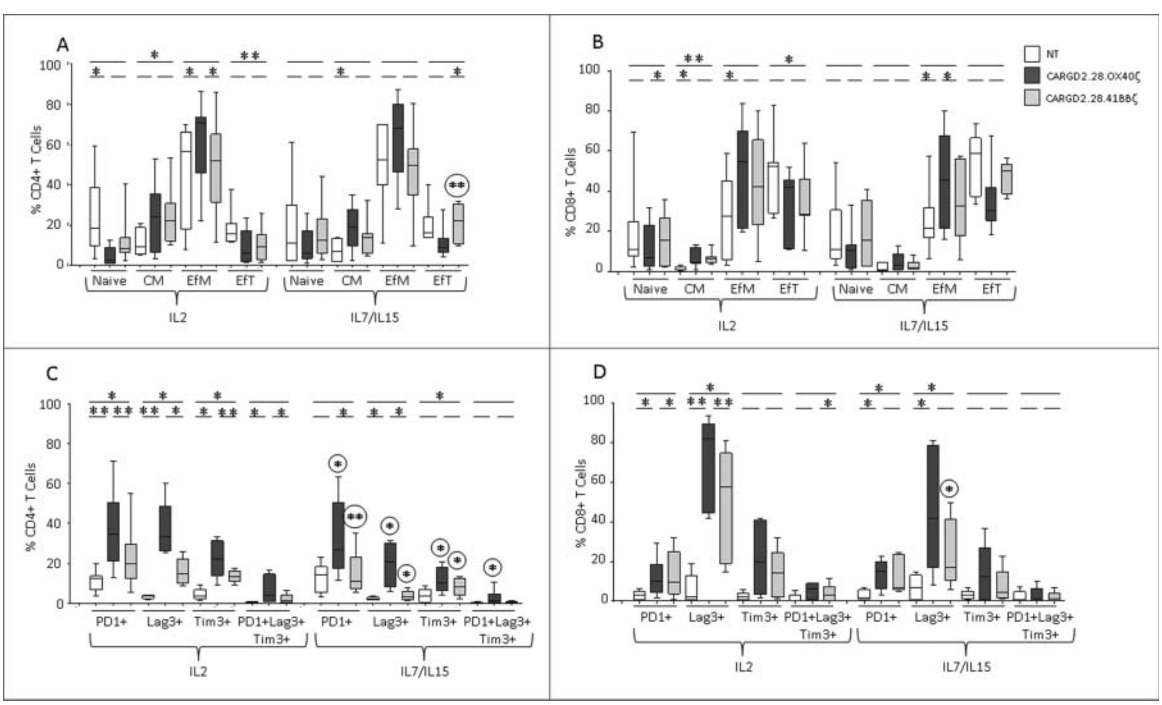

Figure 7. Analysis of $_{III}$CAR.GD2 T cell subsets and of the expression of exhaustion molecules. (A-B) Flow-cytometry analysis of the proportion of *näive*, CM, EfM and EfT subsets of CD4$^+$ (A) or CD8$^+$ (B) T cells, in either NT (white bar), CARGD2.28.4–1BBζ (light gray bar) or CARGD2.28.OX40ζ (dark gray bar), expanded for 15 days in the presence of IL2 or IL7/IL15. Data from 7 HDs are expressed as average ± SD. (C-D) Basal exhaustion profile of CD4$^+$ (C) or CD8$^+$ (D) T cells representative of 7 HDs, in either NT (white bar), CARGD2.28.4–1BBζ (light gray bar) or CARGD2.28.OX40ζ (dark gray bar) expanded for 15 days in the presence of either IL2 (plain colour bars) or IL7/IL15 (tiled bars). The circle around the asterisk(s) indicates the p-value for comparison between the same population of T cells cultured in presence either of IL7/IL15 or IL2. Data from 4 HDs are expressed as average ± SD. *p-value = < 0.05; **p-value = < 0.001; ***p-value = < 0.0001.

immunomodulatory receptors on the CD4$^+$ subpopulation significantly increased compared to NT (Fig. 7C and Supplemental Fig. 7A). When the co-expression of these markers was analysed, the fraction of positive cells was significantly higher in CARGD2.28.OX40ζ, compared to CARGD2.28.4–1BBζ T cells or NT, suggesting a more exhausted profile (Fig. 7C and Supplementary Fig. 7B). Interestingly, in the presence of IL7/IL15, we observed a significant reduction of the exhaustion profile (in terms of PD-1, LAG3 and TIM3 expression) in both CD4$^+$ and CD8$^+$ CARGD2.28.OX40ζ T cells, with loss of the differences between CARGD2.28.OX40ζ and CARGD2.28.4–1BBζ T cells observed in IL2 condition (Fig. 7C–D). However, in the CD4$^+$ CARGD2.28.OX40ζ T cells cultured in presence of IL7/IL15, the expression of Lag3 and PD1 remains significantly higher compared to that observed in CARGD2.28.4–1BBζ T cells, underlining the maintenance of a strongly activated phenotype of this T-cell subpopulation. In co-culture experiments with GD2$^+$ NB cell lines SHSY5Y and IMR-32 (Fig. 8A–C), we confirmed that the presence of an exhaustion profile in CARGD2.28.OX40ζ T cells was significantly higher than in CARGD2.28.4–1BBζ T cells cultured with either IL2 or IL7/IL15. Interestingly, in the co-culture with SHSY5Y GD2(neg) subclone only the CARGD2.28.OX40ζ T cells showed a significant up-regulation of the inhibitory-receptors PD1 and TIM3 (Fig. 8C).

Fine-tuning of cytokines and choice of costimulatory domains influence in vivo *activity of $_{III}$CAR.GD2 T cells*

In view of the *in vitro* data, *in vivo* experiments were performed with $_{III}$CAR.GD2 T cells cultured in IL7/IL15, observing a significant anti-tumor effect with both constructs. While in the NT group, bioluminescence progressively increased over time, mice receiving $_{III}$CAR.GD2 T cells experienced long-term tumor control, with no differences between the two types of $_{III}$CAR.GD2 T cells (Fig. 9A–C). In dedicated experiments, we sacrificed mice at day+25 to evaluate the tumor volume (Fig. 9D). While in the presence of IL2, only CARGD2.28.4–1BBζ T cells were able to significantly control tumor growth compared to both NT and CARGD2.28.OX40ζ T cells, both IL7/IL15 cultured $_{III}$CAR.GD2 T cells showed improved tumor control (Fig. 9E). A significant improvement of DFS was observed in mice treated with CARGD2.28.OX40ζ T cells expanded in IL7/IL15 compared to those expanded with IL2 (Fig. 9G). Although DFS did not differ between mice treated with CARGD2.28.4–1BBζ T cells cultured in the presence of either IL2 or IL7/IL15, only CAR T cells grown in the presence of IL7/IL15 were able to induce a 60-day DFS of 100% in the treated mice (Fig. 9H). These data on the *in vivo* anti-tumor efficacy of CAR T cells correlated with CAR T-cell persistence and expansion. Indeed, the highest percentage of human CD45$^+$/CD3$^+$ cells was found in mice treated with $_{III}$CAR.GD2 T cells produced in the presence of IL7/IL15 (Supplementary Fig. 8 A-B); moreover, the highest percentage of CAR T cells was associated with the CARGD2.28.4–1BBζ construct (Supplementary Fig. 8 C-D). Although we observed a significant different *in vivo* behavior between the two $_{III}$CAR.GD2 T cells, AP1903 treatment was able to eliminate circulating CAR-T cells in both $_{III}$CAR.GD2 T cells (Supplementary Fig. 9 A-C).

Discussion

Clinical trials conducted so far in children with NB using both 1st[17,18] and 3rd (CD28.OX40)[21] generation CARs targeting GD2 have demonstrated only limited efficacy. Nevertheless, important lessons have been learned from these trials, with particular regard to data concerning the improved persistence and efficacy of CAR T cells *in vivo*, as well as the importance of enhancing

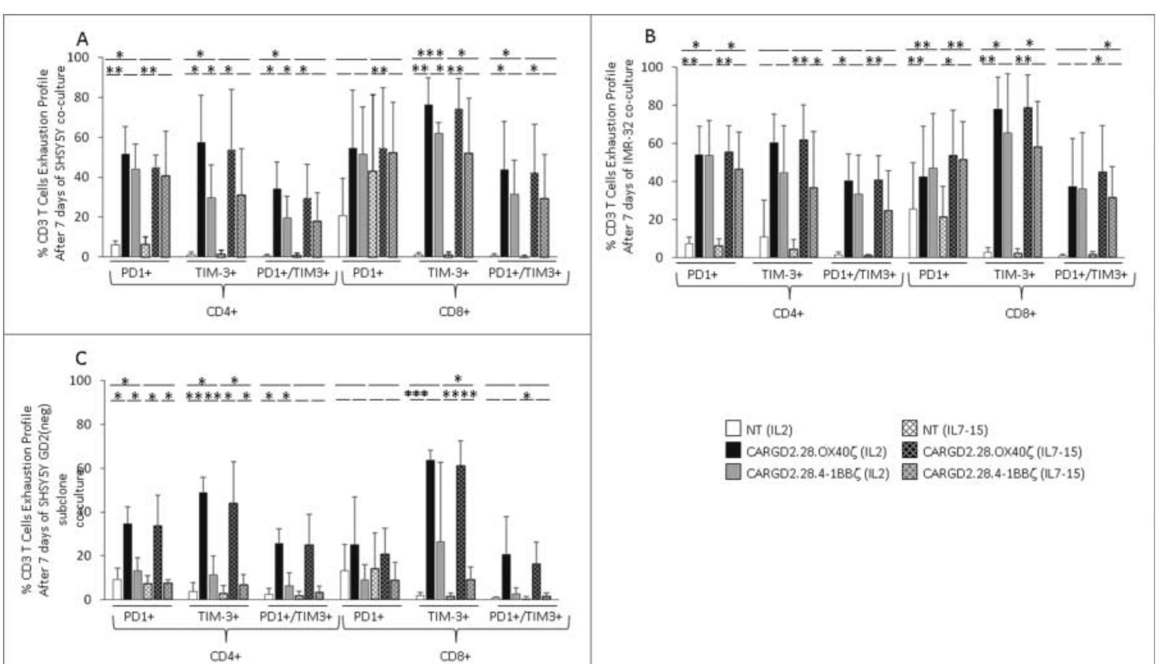

Figure 8. Analysis of $_{III}$CAR.GD2 T cell exhaustion profile after long-term co-culture with NB tumor cell lines. (A-C) Induced exhaustion profile of CD4$^+$ or CD8$^+$ grown in presence of IL2 or IL7/IL15 (tiled bars), in NT (white bar), CARGD2.28.OX40ζ (black bar) and CARGD2.28.4–1BB ζ T cells (gray bar), after 7 days of co-culture with GD2$^+$ SHSY5Y cell line (A), GD2$^+$ IMR-32 cell line (B) or SHSY5Y GD2(neg) subclone (C). Data from 4 HDs are expressed as average ± SD. *p-value = < 0.05; **p-value = < 0.001; ***p-value = < 0.0001.

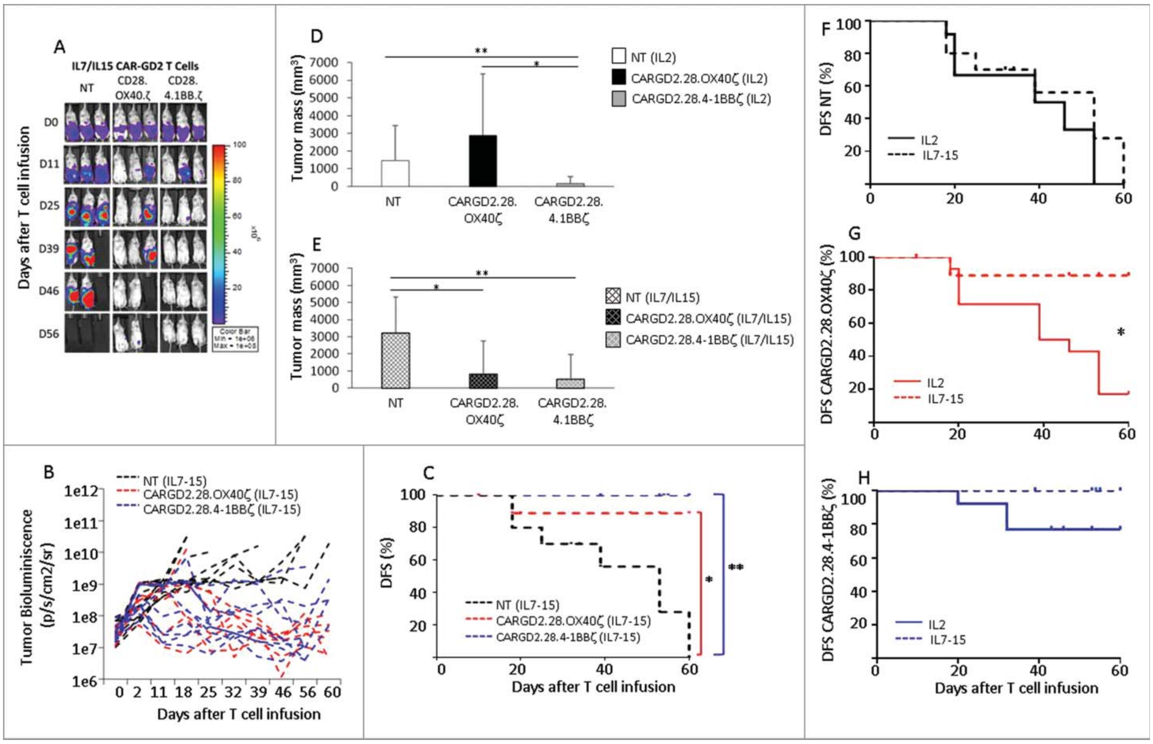

Figure 9. *In vivo* activity of $_{III}$CAR.GD2 T cells generated and expanded in the presence of IL7/IL15. (A-B) *In vivo* bioluminescence imaging of NSG mice bearing i.p. GD2^{+} SHSY5Y-FF-Luc.GFP cells treated with NT, CARGD2.28.OX40ζ or CARGD2.28.4–1BBζ T cells generated and expanded in the presence of IL7/IL15. (A) Bioluminescence imaging of 3 representative mice per group; (B) bioluminescence of each single mouse treated with NT (black line; 10 mice), CARGD2.28.OX40ζ (red line; 10 mice) and CARGD2.28.4–1BBζ T cells (blue line; 10 mice). (C) Kaplan-Meier estimate of DFS in tumor-bearing mice treated with either NT (black line; 10 mice), or CARGD2.28.OX40ζ (red line; 10 mice) or CARGD2.28.4–1BBζ (blue line; 10 mice) T cells (dashed line). (D-E) Tumor mass measured in mice sacrificed after 25 days of treatment with NT (white bar), CARGD2.28.OX40ζ (black bar) and CARGD2.28.4–1BBζ T cells (gray bar) expanded in the presence of IL2, 10 mice per group (D), or IL7/IL15, 10 mice per group (E). (F-H) Kaplan-Meier estimate of DFS of NSG mice bearing i.p. SHSY5Y-FF-Luc.GFP cells after adoptive i.p. transfer of either NT (F), or CARGD2.28.OX40ζ (G) or CARGD2.28.4-1BBζ T cells (H) expanded in presence of IL2 (continuous line) or IL7/IL15 (dashed line). $^{**}p<0.01$ and $^{*}p<0.05$; log-rank (Mantel-Cox). *p-value = <0.05; **p-value = <0.001; ***p-value = <0.0001.

costimulation and reducing T-cell exhaustion.[23] In this study, we documented that $_{III}$CAR.GD2 is able to guarantee a better *in vivo* persistence compared to $_{II}$CAR.GD2. Moreover, our data highlight that there is a clear difference between the two $_{III}$CAR.GD2 constructs that we tested, with a more homogenous and longer T-cell persistence in the group of mice treated with CD28.4-1BB. The high variability of persistence observed in the group of CD28. OX40 treated mice is in agreement with the results observed in the clinical trial reported by Heczey et al.[21]

The role of T-cell exhaustion is particularly relevant in the context of adoptive T-cell therapy for treatment of solid tumors, since it has been clearly shown that expansion and persistence of the adoptively transferred cells are crucial for patient outcome.[6,23,42] The possibility to modulate the degree of T-cell exhaustion, which limits anti-tumor efficacy, remains largely unexplored. Recently, the exhaustion status of CAR-T cells has been associated with the tonic signaling that T cells receive from the framework regions within a specific scFv, as proven in a $_{II}$CAR.GD2 molecule incorporating the 14.G2a-scFv(8). In particular, Long and Colleagues demonstrated an antigen-independent clustering in the presence of CD28, which enhanced development of exhaustion in the setting of chronic CAR.GD2 signaling, but not in the context of CARs with different specificity (i.e. CD19 antigen)(8).

We demonstrated that our $_{III}$CAR.GD2 construct, while incorporating the same scFv and CD28 costimulation, have a substantially different behaviour, probably due to the nature of the second costimulatory domain and to the cytokines used *in vitro*. In particular, 4-1BB signalling does not induce the exhaustion status reported in $_{II}$CAR.GD2 CARGD2.CD28ζ(8). Moreover, we found that 4-1BB was able to rescue the CD28-induced exhaustion observed in our $_{III}$CAR.GD2 construct when OX40 was used as 2nd co-stimulatory domain. In IL2-generated $_{III}$CAR.GD2 T cells, the presence of CD28 in combination with OX40 (CD28.OX40) was associated with higher basal, antigen-independent, *in vitro* proliferation and lower *in vivo* anti-tumor activity than the combination of CD28.4-1BB. In line with the observation that the activation status of CAR-T cells can be related to the cluster distribution of the molecules on T-cell membrane,[43,44] we show that our $_{III}$CAR.GD2 with CD28.OX40 was associated with larger cluster formation and polarization of the immune synapses. A similar pattern was observed in $_{II}$CAR.GD2 with CD28 costimulation alone. By contrast, the presence of 4-1BB was able to revert this effect, inducing a more homogeneous distribution of the CAR molecules.

In order to investigate the basal cellular activation and the physiologic input of receptor clustering in $_{III}$CAR.GD2, we performed a high-throughput phospho-proteomic analysis, which revealed a significantly higher number of phosphorylation sites characterizing CARGD2.28.OX40ζ as compared to CARGD2.28.4-1BBζ T cells. This finding corroborates the hypothesis of T-cell overstimulation mediated by CD28 and not reversed by OX40. In addition, heat-map analysis showed clustered distribution of the involved phosphorylation sites, with a clear unique profile distinguishing the two $_{III}$CAR.GD2 T-cell populations investigated.

All the described features characterizing $_{III}$CAR.GD2 correlated with the exhaustion status associated with the CARGD2.28.OX40ζ construct, as assessed by immune-phenotyping in both resting and antigen-activated CAR-T cells, and explaining the *in vivo* behaviour of CAR-T cells grown in IL2.

To investigate whether cytokines can affect $_{III}$CAR.GD2 T-cell characteristics, we generated and expanded CAR-T cells also in the presence of IL7/IL15. These cytokines are known to enhance survival and proliferation of the stem cell memory population, improving *in vivo* engraftment and persistence of T cells.[45]

As compared to IL2, the combination of IL7/IL15 did not affect *in vitro* the CAR T-cell subpopulation composition, anti-tumor activity or cytokine production upon antigen-specific stimulation.[36,39] Overall, CARGD2.28.4-1BBζ T cells were able to secrete a significantly higher amount of IFNγ than CARGD2.28.OX40ζ. After exposure to GD2$^+$ tumor cells, a higher quantity of IL2 was produced by CARGD2.28.OX40ζ (at day+15 from transduction), due to the signaling of OX40[46,47] and the predominance of CD4$^+$ CAR-T cells in these products.[48] However, when tested on day+30, CARGD2.28.OX40ζ T cells (grown in IL2) displayed a significantly reduced production of IL2 and IFNγ as compared to CARGD2.28.4-1BBζ T cells, this finding correlating with the exhaustion immune profile of CARGD2.28.OX40ζ T cells.

We showed that the use of IL7/IL15 significantly reduces both the individual expression of PD-1, LAG-3 and TIM-3, as well as their co-expression, especially on CD4$^+$ CARGD2.28.OX40ζ T cells, but also in both CD4$^+$ and CD8$^+$ CARGD2.28.4-1BBζ T cells. However, in CD4$^+$ CARGD2.28.OX40ζ T cells, the expression of Lag3 and PD1 remains significantly higher compared to the CARGD2.28.4-1BBζ T cells, this finding being in agreement with the maintenance of a strongly activated phenotype. The exhaustion phenotype well correlated with the observation that IL7/IL15 CARGD2.28.OX40ζ T cells recover the ability of long-term *in vitro* proliferation upon cytokine exposure.

Our results clearly indicate that IL7/IL15 CARGD2.28.4-1BBζ T cells exert the best anti-tumor activity, being able to control tumor cell growth *in vitro* even at an E:T ratio as low as 1:12 (see also Fig. 6). Moreover, these results correlate with the *in vivo* data, since the strongest anti-tumor activity in the NB-xenograft model, were observed when mice were treated with IL7/IL15 CARGD2.28.4-1BBζ T cells. Similarly, IL7/IL15 improved *in vivo* tumor control and expansion of CARGD2.28.OX40ζ T cells. However, further studies evaluating T-cell subsets need to be performed in order to understand the kinetic aspects involved in the T-cell persistence in mice cured from tumor.

The potential risks associated with the acute hyper-inflammatory response mediated by CAR-T cells[27] and with their long-lasting *in vivo* persistence[5] remain a matter of concern in this innovative type of immunotherapy. A strategy for controlling these risks is represented by the inclusion of a safety switch in the construct. Our experimental data show that activation of iC9, successfully included in our construct without impairing neither CAR expression nor anti-tumor T-cell activity (as seen in short and long-term cytotoxicity assays), leads to prompt apoptosis of CAR- T cells, this finding being of relevant utility in a clinical perspective.

In this study, we analyzed one of the key aspects of limited GD2.CAR efficacy: the definition of the optimal CAR design. The clinical trials conducted so far underline that T-cell persistence is a major limiting factor for *in vivo* efficacy of GD2.CAR T-cell therapies.[17,18] Optimization of both CAR costimulation and *in vitro* culture conditions represent key factors influencing the *in vivo* efficacy of this innovative immune-therapeutic approach. The results of this study allowed us to identify the $_{III}$CAR.GD2 construct including iC9 and CD28.4-1BB as the most promising candidate for clinical application. In view of these experimental data, a clinical trial with this vector construct is going to be launched in our Institution to evaluate its safety and efficacy in high-risk NB patients.

Nevertheless, it needs to be noted that this study has been focused on the optimization of GD2.CAR T cells targeting NB cell lines *in vitro* and *in vivo* and results cannot necessarily be translated to constructs with different single chains. Therefore, further studies addressing the definition of the optimal CAR design in other disease models as well as in the context of CARs with a different specificity are needed

Materials and methods

Cell lines. Neuroblastoma (NB)-derived cell lines SHSY5Y, IMR-32 and the leukemia cell line K562 were obtained from LGC Standards-ATCC. We selected the GD2-negative subclone of SHSY5Y [SHSY5Y GD2(neg)] cell line with the BD FACSAria III sorter. The SHSY5Y cell lines were maintained in culture with DMEM medium (Gibco, Invitrogen^{TM}, Carlsbad, CA); the 293 T VEC and the IMR-32 cell line were cultured with IMDM (Gibco; USA), whereas the erythro-leukemia cell line K562 was maintained in RPMI 1640 medium (Gibco; USA). Cell lines were supplemented with 10% fetal bovine serum (FBS, Hyclone, Thermo Scientific, Pittsburgh, PA) and 2 mM GlutaMax (Invitrogen, California, USA). Cells were maintained in a humidified atmosphere containing 5% CO_2 at 37°C. All cell lines were routinely tested for mycoplasma and for surface expression of target antigens. All cell lines have been authenticated by STR analysis in the certificated lab "BMR Genomics s.r.l.".

Retroviral constructs. $_{III}$CAR.GD2 molecules were generated by joining the GD2-specific antibody single chain variable fragment (scFv) 14.G2a,[18,49–51] with the endodomains derived from the T-cell receptor CD3 zeta-chain (ζ) and the costimulatory molecules CD28 and either OX40 (CAR-GD2.CD28.OX40ζ, kindly provided by Prof. Malcolm Brenner) or 4-1BB (CAR-GD2.CD28.4-1BBζ). $_{II}$CAR.GD2 were cloned in order to generate three CARs encoding as costimulatory molecule: CD28, OX40 or 4-1BB. An additional retroviral vector encoding eGFP-Firefly-Luciferase (eGFP-FFLuc) was used in selected experiments to label tumor cells (SHSY5Y-FF-Luc.GFP and IMR-32-FF-Luc.GFP) or T lymphocytes for *in vitro* and *in vivo* studies as previously described(23, 52).

Isolation, generation and transduction of effector cells. Peripheral blood mononuclear cells (PBMC) were isolated from buffy coats obtained from healthy donors (OPBG Hospital, Rome, Italy) who signed a written informed consent, in accordance with rules set by the Institutional Review Board of OPBG (Approval of Ethical Committee N°969/2015 prot. N° 669LB), using Lymphocytes separation medium (Eurobio; France). T lymphocytes were activated with immobilized OKT3 (1 μg/ml, e-Bioscience Inc.;San Diego, CA, USA) and anti-CD28 (1 μg/ml, BD Biosciences, Europe) monoclonal antibody (mAb) in the presence of recombinant human interleukin-2 (IL2, 100 U/ml; R&D; USA)(52), or with a combination of recombinant human interleukin-7 (IL7, 10 ng/ml; R&D; USA) and 15 (IL15, 5 ng/ml; R&D).[35,37,38] Activated T cells were transduced on day 3 in 24-well plates pre-coated with recombinant human RetroNectin (Takara-Bio. Inc; Japan) using a specific retroviral supernatant and the specific above-described cytokines. On day 5 after transduction, T cells were expanded in medium containing 45% RPMI1640 and 45% Click's medium (Sigma-Aldrich, Co.; USA) supplemented with 10% FBS and 2 mM Glutamax, and replenished twice a week.

Phenotypic analysis. Expression of cell surface molecules was determined by flow-cytometry using standard methodology. The following mAbs were used: CD3, CD4, CD8, CD25, CD27, CD28, CD45RA, CD45RO, CD56, CD57, CD62 L, CD62E, CD62P, CD95, CD106, CD127, CD137, CD197, CD223 (Lag3), CD274 (PDL1), CD279 (PD1), and TIM3. The expression of GD2 antigen on tumor cell lines was assessed with an anti-GD2 mAb (clone 14.G2a, BD).[23] The expression of CAR.GD2 on T cells was detected using a specific anti-idiotype antibody (1A7). T-cell receptor (TCR)-Vβ repertoire on NT and CAR-T cells, was evaluated at day+15 and day+30, using a panel of 24 different TCR Vβ- specific mAbs (IO TEST Beta Mark TCR-Vβ repertoire kit, BC) used in association with CD3 specific mAb (BD Biosciences) and isotype control (BD Biosciences).[53] Samples were analyzed with a BD LSRFortessa X-20. Data were analyzed using the FACS-Diva software (BD Biosciences). For each sample, we analyzed a minimum of 20,000 events.

Chromium release assay. The cytotoxic activity was evaluated using a 6-hour ^{51}Cr release assay as previously described.[54] Target cells were: SHSY5Y (GD2 = 99.9%), IMR-32 (GD2 = 99.0%), GD2(neg)SHSY5Y and K562 cell line (GD2 = 0%). ^{51}Cr labeled target cells incubated in medium alone or 1% Triton X-100 were used to determine spontaneous and maximal ^{51}Cr release, respectively. After 6 hours of co-culture between effector and target cells, the supernatant was collected and the radioactivity measured with a gamma counter. The mean percentage of specific lysis of triplicate wells was calculated as follows: [(Experimental release-spontaneous release)/(maximal release-spontaneous release)] × 100.

Co-culture assay. For co-culture experiments, NT and CAR. GD2 T lymphocytes were plated at 1×10^6 cells/well in 24-well plates at the indicated E:T ratios. Following 7 days of incubation at 37°C, adherent tumor cells and T cells were collected and residual tumor cells and T cells assessed by fluorescence-activated cell-sorting (FACS) analysis based on CD3 expression (Effector T cells) and GFP (NB tumor GD2$^+$ cell line) or CD45$^-$/CD3$^-$ (NB tumor GD2(neg) cell line), respectively(6, 55).

Cytokine profile. Supernatant from co-cultures was collected at 24 hours to measure cytokine release. Cytokines were measured by MILLIPLEX MAP Human Th17 Magnetic Bead Panel assay (Millipore), using a MAGPIX® with xPONENT® software, following the manufacturer's instructions. In particular, we investigated the following cytokines: IL1β, IL2, IL4, IL5, IL6, IL9, IL10, IL12p70, IL13, IL15, IL17 A, IL17E/IL25, IL17 F, IL21, IL22, IL23, IL27, IL28 A, IL31, IL33, GM-CSF, IFNγ, MIP3 a, TNFα and TNFβ.

Confocal Laser Microscopy and live cell imaging. Cells were collected and washed twice with PBS supplemented with 1% of BSA. CAR expression on T cells was detected by incubation of T cells for 60 minutes at +4°C with a specific anti-idiotype mouse anti-human antibody (1A7) (4 μg/ml), followed by AlexaFluor488-conjugated goat anti-mouse secondary antibody (1:500 in 1% BSA/PBS, Life Technologies) for 60 minutes at +4°C. The cells were seeded and dried on positively-charged slides, then fixed in ice-cold 4% paraformaldehyde (Sigma-Aldrich), washed with PBS and permeabilized with 0.025% Triton X-100 (5 min). Wheat germ agglutinin (WGA) conjugated to AlexaFluor555-conjugated (1:200 in 1% BSA/PBS, Life Technologies) was used as a plasma membrane marker. Nuclei were counterstained with DRAQ5 probe (1:5000 in 1% BSA/PBS, Bio Status). Confocal microscopy imaging was performed by Leica TCS-SP8X laser-scanning confocal microscope (Leica Microsystems) equipped with tunable white light laser source, 405 nm diode laser, 3 (PMT) e 2 (HyD) internal spectral detector channels. Sequential confocal images were acquired using a HC PLAPO 63x oil immersion objective (1.40 numerical aperture, Leica Microsystems) with a 1024 × 1024 image format, scan speed 400 Hz and z-step size of 0.25 μm. Z-reconstructions were imported into IMARIS (Bitplane, Zurich, CH) software to obtain their 3D surface rendering. Three different areas were randomly selected and n = 10 cells were analysed to obtain their volumetric data for each distribution group. Volumes of CAR sites were individually isolated in space and isosurfaces have been built defining the size of individual voxels equal to 0.1 × 0.1 × 0.25 μm, whereas volumes of WGA labelled cells have been built using the 0.2 × 0.2 × 0.25 μm voxel size. Then, total volume of CAR isosurfaces and total cell volume were measured respectively for each cell, and the CAR volumes/cell volume ratio was obtained.[56]

For the time-lapse experiments, SHSY5Y GFP/GD2$^+$ NB tumor cell line was co-cultured with $_{III}$CAR.GD2-modified T cells and analyzed by live imaging during the first 3 hours. To detect the interaction sites between tumor cell line and the $_{III}$CAR.GD2 T cells, Sir-actin probe was added to the medium at final concentration of 0.25 nM (Tebu-bio) at the time of co-culture set-up. During live imaging, cells were maintained in a stage incubator (OkoLab, Naples, Italy) at stable conditions of temperature, CO_2 and humidity. Three-dimensional surface rendering of time-lapse experiments was performed using LASX 3D analysis (Leica Microsystem) software. Tables of images were processed using Adobe Photoshop CS6 software (Adobe Systems Inc).

Phosphoproteome sample preparation. $_{III}$CAR.GD2 T cells were generated as previously indicated and FACS-sorted for the subfraction of CAR$^+$/CD8$^+$ or CAR$^+$/CD4$^+$ T cells. After 10 days of *in vitro* reactivation in the presence of IL2, CAR-T cells were maintained in resting condition for four days. Then, the obtained cells were *in vitro* activated by the exposition to 1 μg/ml of 1A7 activating mAb for 15 minutes. CAR-T cells were subsequently washed in cold PBS before pellet preparation. The cells were lysed, solubilized, denatured and reduced using a solution of 6M GdmCl, 10 mM TCEP, 40 mM CAA, 100 mM Tris pH 8.5. Afterward, the samples were loaded into a 30 kDa filtration devices and mixtures of sequencing grade of Lys C and Trypsin were added at a ratio of 1:50 and 1:100 (μg enzyme: μg protein), respectively. After an overnight digestion at 37°C, peptides were collected with one wash of 50% CH_3OH, 45% H_2O, 5% TFA. After this step, the phosphopeptides were enriched and then purified, following the guidelines outlined in Titansphere Phos-TiO kit (GL Sciences Cat. No. 5010–21312). The enrichment samples were acidified and desalted on C18 StageTips before injection to mass spectrometry.

LC-MS/MS Analysis and Data Processing. The peptide mixtures were separated on an Easy-Spray C18 LC column (75-μm ID × 50 cm, 2 μm, 100 Å) thermostated at 55°C with a non-linear gradient of 2–60% solution B (80% CAN and 20% H_2O, 5% DMSO, 0.1% FA) in 180 min with a flow rate of 250 nl/min. The Dionex UltiMate 3000 Rapid Separation LC system was coupled to an Orbitrap Velos mass spectrometer (Thermo Fisher Scientific) operating in positive ionization mode. Single MS survey scans were performed in the Orbitrap, recording a mass window between 350 and 1650 m/z using a maximum injection time of 250 ms. The resolution was set to 30000 and the automatic gain control was set to 1000000 ions. The most ten prominent ions were fragmented with Collision Induced Dissociation (target value 5000 ions, maximum injection time 150 ms, normalized collision energy of 35%, Q-value 0.25, activation time 10 ms) and detected in Ion Trap. The phosphopeptides were analyzed by automated data-dependent MSA acquisition. The neutral loss species resulting from phosphate loss at 98.5, 65.3, 49.0, 32.7 and 24.5 m/z below the precursor ion are the triggering elements. The MSA event was repeated for the top three ions in a data-dependent mode. Raw MS files were processed with MaxQuant software (version 1.5.3.30, http://coxdocs.org/doku.php?id = maxquant:start)[57] using the integrated Andromeda search engine with a FDR <0.01 for the identification of proteins, peptide and PSM (peptide-spectrum match). A minimum length of 6 amino acids was required for the identification and the "*match between runs*" was enabled with a matching time window of 0.7 min to transfer MS1 identifications between runs. The database used by the software is human (UniProt Release 2016_02) and the digestion enzyme is trypsin. Cysteine carbamidomethylation was selected as fixed modification, whereas acetylation protein N-terminal methionine oxidation, deamidation (N, Q) and phosphorylation (S, T, Y) have been selected as variable modifications. The maximum mass deviation has been set to 7 ppm and 0.5 Da for the precursor ion in MS1 and fragments in MS2 events respectively. The mass spectrometry proteomics data have been deposited to the ProteomeXchange Consortium via the PRIDE[58] partner repository with the dataset identifier PXD005426 (Reviewer account details: *Username*: reviewer46024@ebi.ac.uk, Password: RaHH8xS2).

Western Blot Analysis. Cell lysates were lysed on sodium dodecyl sulfate–polyacrylamide gel electrophoresis. CD3 zeta (phospho Y83) was detected using a rabbit monoclonal antibody [EP776(2)Y] to CD3 zeta (phospho Y83) (ab68236; AbCAM Inc). CD3 zeta was detected using a rabbit monoclonal antibody anti-CD3 zeta antibody [EP286Y] (ab40804; AbCAM Inc). Immunoblots were developed using enhanced chemiluminescence detection reagents (Amersham Biosciences). To evaluate the equal loading of the proteins, membranes were re-probed with Beta-Actin (β-Actin C4) using a mouse monoclonal antibody (mAb; sc-47778; Santa Cruz Biotechnology).

Bioinformatic. For the Venn diagram, numbers represent the distinct phosphorylation sites in the respective overlapping and non-overlapping areas. The normalized intensities in ProfilePlot are the log2 (phosphosite ratio normalized activated on basal of the same $_{III}$CAR.GD2). Heat map shows average log2 values of phosphosite intensities after a normalization process. The log2 values of the intensities were Z-scored for graphical representation. The network was built through the merge between a first network obtained according to ClueGO setup and a second one built by GENEMANIA app of Cytoscape environment, starting from a t-test significant phosphosites matrix that is reduced at the protein level, collapsing the gene identifier. Each big node represents a Gene Ontology Biological Process term or a Reactome pathway, while the small node represents query proteins used for the analysis. The node size represents the P-value obtained from two-sided hypergeometric test corrected by the Bonferroni step-down method. The protein color scheme is associated with the group belonging, red means CARGD2.28.4-1BBζ T cells and blue CARGD2.28.OX40ζ T cells. The same colors are used for the node terms, in which the pie represents the percentage of protein of each group.

Xenograft mouse model for *in vivo* studies. To investigate the *in vivo* antitumor activity of CAR.GD2 T cells, 0.75 × 10^6 $GD2^+$ SHSY5Y-FF-Luc.GFP were intraperitoneally injected (i.p.), in 5 week old NOD.Cg-Prkdc^{scid} Il2rg^{tm1Wjl}/SzJ male mice (Charles River). After engraftment, mice received an intravenous injection (i.v.) of 15 × 10^6 of NT or genetically modified T cells. Tumor growth was evaluated using IVIS imaging system (Xenogen). In this model, we considered the mouse to be in disease-free survival (DFS) if the bioluminescence signal was inferior to 1 × 10^9 p/s/cm^2/sr and the animal was free of any sufferance sign. Briefly, a constant region of interest was drawn over the mouse and the intensity of the signal measured as total photon/sec/cm^2/sr (p/s/cm^2/sr), as previously described.[59,60] All *in vivo* experiments were conducted in compliance with the ethical international, EU and national requirements and were approved by the Italian Health Ministry (N°88/2016-PR).

Administration of the dimerizing drug AP1903 to induce the activation of the safety switch iC9

$_{III}$CAR.GD2 T cells were exposed to 20 nM AP1903 (Kindly provided by Bellicum Pharmaceuticals, Inc.) for 24 hours and residual viable cells were stained with Annexin-V/7AAD (BD Pharmingen) and analysed by FACS analysis. To investigate the *in vivo* activity of AP1903, 0.75 × 10^6 $GD2^+$ SHSY5Y were intraperitoneally injected (i.p.) in 5 week old NOD.Cg-Prkdc^{scid} Il2rg^{tm1Wjl}/SzJ male mice (Charles River). After engraftment, mice received an intravenous injection (i.v.) of 12 × 10^6 of NT or genetically modified T cells. Ten days later, when the presence of circulating T cells was confirmed by FACS analysis, mice were treated twice (on day+11 and day+12) with 100 mg/mouse (i.p.) of AP1903 and residual CAR-T cells were evaluated 4 days later.

Statistical Analysis. Unless otherwise noted, data are expressed as average ± standard deviation (SD). Student *t*-test (two-sided) was used to determine statistically significant differences between samples; a *p* value <0.05 was considered to be statistically significant. When multiple comparison analyses were required, statistical significance was evaluated by a repeated measures ANOVA followed by a Log-rank (Mantel-Cox) test for multiple comparisons. The mouse survival data were analyzed using the Kaplan-Meier survival curves; the log-rank test was used to measure differences between groups. No valuable samples were excluded from the analyses. Animals were excluded only in the event of death after tumor implant, but before T-cell infusion. Neither randomization nor blinding was done during the *in vivo* study. However, mice were matched based on the tumor signal for control and treatment groups before infusion of control or gene-modified T cells. To compare the growth of tumors over time, bioluminescence signal intensity was collected in a blind fashion. Bioluminescence signal intensity was log transformed and then compared using a two-sample t-test. The analysis of the pathologist, aimed at quantifying tumor volume, was performed in a blind fashion. Label-free Quantification (LFQ) experiments were statistically evaluated with Perseus software (http://www.perseus-framework.org)(61). Briefly, the intensities in every sample were normalized by subtracting the median of all the intensities in each sample. Afterwards, the phosphosites were filtered to require 100% valid values in at least one group. The missing values were imputed by drawing random numbers from a normal distribution shifted to simulate signals from low abundant phosphosites. All t-test FDR value <.05 and S0>0.3 were considered statistically significant.

We estimated the sample size considering the variation and average of the samples. We tried to reach a conclusion using a sample size as small as possible. We estimated the sample size to detect a difference in averages of 2 standard deviations at the 0.05 level of significance with an 80% power. Graph generation and statistical analyses were performed using Prism version 6.0 d software (GraphPad, La Jolla, CA).

Disclosure of potential conflicts of interest

No potential conflicts of interest were disclosed.

Acknowledgments

This work was partly supported by grants from: AIRC (Associazione Italiana Ricerca sul Cancro, Special Grant “5xmille”-9962 and Investigator Grant to F. Locatelli; Start-up grant to I. Caruana), Ministero della Salute (RF-2010-2316606 to F. Locatelli; Ricerca Corrente to F. Locatelli, C. Quintarelli, B. De Angelis, I. Caruana). Fondazione Neuroblastoma (CAR T-cell project, F. Locatelli), Regione Lazio (Grant FILAS to F. Locatelli), AIFA (Agenzia Italiana del Farmaco, project 2016–02364631). We thank Igor Paron, Department of Proteomics and Signal Transduction, Max Planck Institute of Biochemistry, Martinsried, Germany, for MS technical advices. We thank Prof. Malcolm K. Brenner (and his research group) for providing the original vector CARGD2.28.OX40ζ, and for his mentorship in the field of CAR immunotherapy

Funding

Associazione Italiana per la Ricerca sul Cancro, Associazione Italiana per la Ricerca sul Cancro, Start-up grant 17184, Ministero della Salute, RF-2010-2316606, Ricerca Corrente, Fondazione Neuroblastoma, Regione Lazio.

Author contributions

B.D.A. and I.C. share last authorship, and C.Q. and F.L. share corresponding authorship of this paper.
C.Q., F.L., B.D.A. and I.C. designed experimental studies, supervised the project conduction, analyzed the data and wrote the manuscript.
D.O., I.B., M.G., F.D.B., V.A.P. performed the *in vitro* and *in vivo* experiments.
A.P. and C.L. conducted LC-MS/MS experiments and analyzed data.
M.S., E.G. and M.S. conducted the immunofluorescence experiments, analyzing results.
S.P. performed Confocal Microscopy analyses.
F.D.B., G.W., and D.P. contributed to the study design and to the analysis of experimental data.

ORCID

Vinicia Assunta Polito http://orcid.org/0000-0002-5698-7778
Biagio De Angelis http://orcid.org/0000-0002-7938-737X
Ignazio Caruana http://orcid.org/0000-0002-9250-0605

References

1. Kershaw MH, Westwood JA, Parker LL, Wang G, Eshhar Z, Mavroukakis SA, White DE, Wunderlich JR, Canevari S, Rogers-Freezer L, et al. A phase I study on adoptive immunotherapy using gene-modified T cells for ovarian cancer. Clin Cancer Res. 2006;12(20 Pt 1):6106–15. doi:10.1158/1078-0432.CCR-06-1183. PMID:17062687.
2. Park JR, Digiusto DL, Slovak M, Wright C, Naranjo A, Wagner J, Meechoovet HB, Bautista C, Chang WC, Ostberg JR, et al. Adoptive transfer of chimeric antigen receptor re-directed cytolytic T lymphocyte clones in patients with neuroblastoma. Mol Ther. 2007;15(4):825–33. doi:10.1038/sj.mt.6300104. PMID:17299405.
3. Till BG, Jensen MC, Wang J, Qian X, Gopal AK, Maloney DG, Lindgren CG, Lin Y, Pagel JM, Budde LE, et al. CD20-specific adoptive immunotherapy for lymphoma using a chimeric antigen receptor with both CD28 and 4-1BB domains: pilot clinical trial results. Blood. 2012;119(17):3940–50. doi:10.1182/blood-2011-10-387969. PMID:22308288.
4. Lamers CH, Sleijfer S, van Steenbergen S, van Elzakker P, van Krimpen B, Groot C, Vulto A, den Bakker M, Oosterwijk E, Debets R, et al. Treatment of metastatic renal cell carcinoma with CAIX CAR-engineered T cells: clinical evaluation and management of on-target toxicity. Mol Ther. 2013;21(4):904–12. doi:10.1038/mt.2013.17. PMID:23423337.
5. Maude SL, Frey N, Shaw PA, Aplenc R, Barrett DM, Bunin NJ, Chew A, Gonzalez VE, Zheng Z, Lacey SF, et al. Chimeric antigen receptor T cells for sustained remissions in leukemia. N Engl J Med. 2014;371(16):1507–17. doi:10.1056/NEJMoa1407222. PMID:25317870.
6. Caruana I, Savoldo B, Hoyos V, Weber G, Liu H, Kim ES, Ittmann MM, Marchetti D, and Dotti G. Heparanase promotes tumor infiltration and antitumor activity of CAR-redirected T lymphocytes. Nat Med. 2015;21(5):524–9. doi:10.1038/nm.3833. PMID:25849134.
7. Long AH, Highfill SL, Cui Y, Smith JP, Walker AJ, Ramakrishna S, El-Etriby R, Galli S, Tsokos MG, Orentas RJ, et al. Reduction of MDSCs with All-trans Retinoic Acid Improves CAR Therapy Efficacy for Sarcomas. Cancer Immunol Res. 2016;4(10):869–80. doi:10.1158/2326-6066.CIR-15-0230. PMID:27549124.
8. Long AH, Haso WM, Shern JF, Wanhainen KM, Murgai M, Ingaramo M, Smith JP, Walker AJ, Kohler ME, Venkateshwara VR, et al. 4-1BB costimulation ameliorates T cell exhaustion induced by tonic signaling of chimeric antigen receptors. Nat Med. 2015;21(6):581–90. doi:10.1038/nm.3838. PMID:25939063.

9. Hegde M, Mukherjee M, Grada Z, Pignata A, Landi D, Navai SA, Wakefield A, Fousek K, Bielamowicz K, Chow KK, et al. Tandem CAR T cells targeting HER2 and IL13Ralpha2 mitigate tumor antigen escape. J Clin Invest. 2016;126(8):3036–52. doi:10.1172/JCI83416. PMID:27427982.
10. Kushner BH, Kramer K, Modak S, and Cheung NK. Successful multifold dose escalation of anti-GD2 monoclonal antibody 3F8 in patients with neuroblastoma: a phase I study. J Clin Oncol. 2011;29(9):1168–74. doi:10.1200/JCO.2010.28.3317. PMID:21343563.
11. Modak S, and Cheung NK. Disialoganglioside directed immunotherapy of neuroblastoma. Cancer Invest. 2007;25(1):67–77. doi:10.1080/07357900601130763. PMID:17364560.
12. Yu AL, Gilman AL, Ozkaynak MF, London WB, Kreissman SG, Chen HX, Smith M, Anderson B, Villablanca JG, Matthay KK, et al. Anti-GD2 antibody with GM-CSF, interleukin-2, and isotretinoin for neuroblastoma. N Engl J Med. 2010;363(14):1324–34. doi:10.1056/NEJMoa0911123. PMID:20879881.
13. Robbins PF, Dudley ME, Wunderlich J, El-Gamil M, Li YF, Zhou J, Huang J, Powell DJ, Jr., and Rosenberg SA. Cutting edge: persistence of transferred lymphocyte clonotypes correlates with cancer regression in patients receiving cell transfer therapy. J Immunol. 2004;173(12):7125–30. doi:10.4049/jimmunol.173.12.7125. PMID:15585832.
14. Kowolik CM, Topp MS, Gonzalez S, Pfeiffer T, Olivares S, Gonzalez N, Smith DD, Forman SJ, Jensen MC, and Cooper LJ. CD28 costimulation provided through a CD19-specific chimeric antigen receptor enhances in vivo persistence and antitumor efficacy of adoptively transferred T cells. Cancer Res. 2006;66(22):10995–1004. doi:10.1158/0008-5472.CAN-06-0160. PMID:17108138.
15. Milone MC, Fish JD, Carpenito C, Carroll RG, Binder GK, Teachey D, Samanta M, Lakhal M, Gloss B, Danet-Desnoyers G, et al. Chimeric receptors containing CD137 signal transduction domains mediate enhanced survival of T cells and increased antileukemic efficacy in vivo. Mol Ther. 2009;17(8):1453–64. doi:10.1038/mt.2009.83. PMID:19384291.
16. Haso W, Lee DW, Shah NN, Stetler-Stevenson M, Yuan CM, Pastan IH, Dimitrov DS, Morgan RA, FitzGerald DJ, Barrett DM, et al. Anti-CD22-chimeric antigen receptors targeting B-cell precursor acute lymphoblastic leukemia. Blood. 2013;121(7):1165–74. doi:10.1182/blood-2012-06-438002. PMID:23243285.
17. Louis CU, Savoldo B, Dotti G, Pule M, Yvon E, Myers GD, Rossig C, Russell HV, Diouf O, Liu E, et al. Antitumor activity and long-term fate of chimeric antigen receptor-positive T cells in patients with neuroblastoma. Blood. 2011;118(23):6050–6. doi:10.1182/blood-2011-05-354449. PMID:21984804.
18. Pule MA, Savoldo B, Myers GD, Rossig C, Russell HV, Dotti G, Huls MH, Liu E, Gee AP, Mei Z, et al. Virus-specific T cells engineered to coexpress tumor-specific receptors: persistence and antitumor activity in individuals with neuroblastoma. Nat Med. 2008;14(11):1264–70. doi:10.1038/nm.1882. PMID:18978797.
19. Heslop HE. Safer CARS. Mol Ther. 2010;18(4):661–2. doi:10.1038/mt.2010.42. PMID:20357776.
20. Sadelain M, Brentjens R, and Riviere I. The promise and potential pitfalls of chimeric antigen receptors. Curr Opin Immunol. 2009;21(2):215–23. doi:10.1016/j.coi.2009.02.009. PMID:19327974.
21. Heczey A, Louis CU, Savoldo B, Dakhova O, Durett A, Grilley B, Liu H, Wu MF, Mei Z, Gee A, et al. CAR T Cells Administered in Combination with Lymphodepletion and PD-1 Inhibition to Patients with Neuroblastoma. Mol Ther. 2017;25(9):2214–24. doi:10.1016/j.ymthe.2017.05.012. PMID:28602436.
22. Gomes da Silva D, Mukherjee M, Srinivasan M, Dakhova O, Liu H, Grilley B, Gee AP, Neelapu SS, Rooney CM, Heslop HE, et al. Direct Comparison of In Vivo Fate of Second and Third-Generation CD19-Specific Chimeric Antigen Receptor (CAR)-T Cells in Patients with B-Cell Lymphoma: Reversal of Toxicity from Tonic Signaling. Blood. 2016;128(22):1851.
23. Caruana I, Weber G, Ballard BC, Wood MS, Savoldo B, and Dotti G. K562-Derived Whole-Cell Vaccine Enhances Antitumor Responses of CAR-Redirected Virus-Specific Cytotoxic T Lymphocytes In Vivo. Clin Cancer Res. 2015;21(13):2952–62. doi:10.1158/1078-0432.CCR-14-2998. PMID:25691731.
24. Savoldo B, Ramos CA, Liu E, Mims MP, Keating MJ, Carrum G, Kamble RT, Bollard CM, Gee AP, Mei Z, et al. CD28 costimulation improves expansion and persistence of chimeric antigen receptor-modified T cells in lymphoma patients. J Clin Invest. 2011;121(5):1822–6. doi:10.1172/JCI46110. PMID:21540550.
25. Hombach AA, and Abken H. Costimulation by chimeric antigen receptors revisited the T cell antitumor response benefits from combined CD28-OX40 signalling. Int J Cancer. 2011;129(12):2935–44. doi:10.1002/ijc.25960. PMID:22030616.
26. Song DG, Ye Q, Carpenito C, Poussin M, Wang LP, Ji C, Figini M, June CH, Coukos G, and Powell DJ, Jr. In vivo persistence, tumor localization, and antitumor activity of CAR-engineered T cells is enhanced by costimulatory signaling through CD137 (4–1BB). Cancer Res. 2011;71(13):4617–27. doi:10.1158/0008-5472.CAN-11-0422. PMID:21546571.
27. Brudno JN, and Kochenderfer JN. Toxicities of chimeric antigen receptor T cells: recognition and management. Blood. 2016;127(26):3321–30. doi:10.1182/blood-2016-04-703751. PMID:27207799.
28. Maude SL, Barrett D, Teachey DT, and Grupp SA. Managing cytokine release syndrome associated with novel T cell-engaging therapies. Cancer J. 2014;20(2):119–22. doi:10.1097/PPO.0000000000000035. PMID:24667956.
29. van den Berg JH, Gomez-Eerland R, van de Wiel B, Hulshoff L, van den Broek D, Bins A, Tan HL, Harper JV, Hassan NJ, Jakobsen BK, et al. Case Report of a Fatal Serious Adverse Event Upon Administration of T Cells Transduced With a MART-1-specific T-cell Receptor. Mol Ther. 2015;23(9):1541–50. doi:10.1038/mt.2015.60. PMID:25896248.
30. Gust J, Hay KA, Hanafi LA, Li D, Myerson D, Gonzalez-Cuyar LF, Yeung C, Liles WC, Wurfel M, Lopez JA, et al. Endothelial Activation and Blood-Brain Barrier Disruption in Neurotoxicity after Adoptive Immunotherapy with CD19 CAR-T Cells. Cancer Discov. 2017;7(12):1404–1419. doi:10.1158/2159-8290.CD-17-0698. PMID:29025771.
31. Turtle CJ, Hanafi LA, Berger C, Hudecek M, Pender B, Robinson E, Hawkins R, Chaney C, Cherian S, Chen X, et al. Immunotherapy of non-Hodgkin's lymphoma with a defined ratio of CD8+ and CD4+ CD19-specific chimeric antigen receptor-modified T cells. Sci Transl Med. 2016;8(355):355ra116. doi:10.1126/scitranslmed.aaf8621. PMID:27605551.
32. Brown CE, Badie B, Barish ME, Weng L, Ostberg JR, Chang WC, Naranjo A, Starr R, Wagner J, Wright C, et al. Bioactivity and Safety of IL13Ralpha2-Redirected Chimeric Antigen Receptor CD8+ T Cells in Patients with Recurrent Glioblastoma. Clin Cancer Res. 2015;21(18):4062–72. doi:10.1158/1078-0432.CCR-15-0428. PMID:26059190.
33. Hoyos V, Savoldo B, Quintarelli C, Mahendravada A, Zhang M, Vera J, Heslop HE, Rooney CM, Brenner MK, and Dotti G. Engineering CD19-specific T lymphocytes with interleukin-15 and a suicide gene to enhance their anti-lymphoma/leukemia effects and safety. Leukemia. 2010;24(6):1160–70. doi:10.1038/leu.2010.75. PMID:20428207.
34. Karlsson H, Svensson E, Gigg C, Jarvius M, Olsson-Stromberg U, Savoldo B, Dotti G, and Loskog A. Evaluation of Intracellular Signaling Downstream Chimeric Antigen Receptors. PLoS One. 2015;10(12):e0144787. doi:10.1371/journal.pone.0144787. PMID:26700307.
35. Perna SK, De Angelis B Pagliara D, Hasan ST, Zhang L, Mahendravada A, Heslop HE, Brenner MK, Rooney CM, Dotti G, et al. Interleukin 15 provides relief to CTLs from regulatory T cell-mediated inhibition: implications for adoptive T cell-based therapies for lymphoma. Clin Cancer Res. 2013;19(1):106–17. doi:10.1158/1078-0432.CCR-12-2143. PMID:23149818.
36. Cieri N, Camisa B, Cocchiarella F, Forcato M, Oliveira G, Provasi E, Bondanza A, Bordignon C, Peccatori J, Ciceri F, et al. IL-7 and IL-15 instruct the generation of human memory stem T cells from naive precursors. Blood. 2013;121(4):573–84. doi:10.1182/blood-2012-05-431718. PMID:23160470.
37. Perna SK, Pagliara D, Mahendravada A, Liu H, Brenner MK, Savoldo B, and Dotti G. Interleukin-7 mediates selective expansion of tumor-redirected cytotoxic T lymphocytes (CTLs) without enhancement of regulatory T-cell inhibition. Clin Cancer Res. 2014;20(1):131–9. doi:10.1158/1078-0432.CCR-13-1016. PMID:24097874.

38. Gargett T, and Brown MP. Different cytokine and stimulation conditions influence the expansion and immune phenotype of third-generation chimeric antigen receptor T cells specific for tumor antigen GD2. Cytotherapy. 2015;17(4):487–95. doi:10.1016/j.jcyt.2014.12.002. PMID:25573334.
39. Xu Y, Zhang M, Ramos CA, Durett A, Liu E, Dakhova O, Liu H, Creighton CJ, Gee AP, Heslop HE, et al. Closely related T-memory stem cells correlate with in vivo expansion of CAR.CD19-T cells and are preserved by IL-7 and IL-15. Blood. 2014;123(24):3750–9. doi:10.1182/blood-2014-01-552174. PMID:24782509.
40. Zaph C, Du Y, Saenz SA, Nair MG, Perrigoue JG, Taylor BC, Troy AE, Kobuley DE, Kastelein RA, Cua DJ, et al. Commensal-dependent expression of IL-25 regulates the IL-23-IL-17 axis in the intestine. J Exp Med. 2008;205(10):2191–8. doi:10.1084/jem.20080720. PMID:18762568.
41. Iwakura Y, and Ishigame H. The IL-23/IL-17 axis in inflammation. J Clin Invest. 2006;116(5):1218–22. doi:10.1172/JCI28508. PMID: 16670765.
42. Porter DL, Hwang WT, Frey NV, Lacey SF, Shaw PA, Loren AW, Bagg A, Marcucci KT, Shen A, Gonzalez V, et al. Chimeric antigen receptor T cells persist and induce sustained remissions in relapsed refractory chronic lymphocytic leukemia. Sci Transl Med. 2015;7 (303):303ra139. doi:10.1126/scitranslmed.aac5415. PMID:26333935.
43. Dolezal O, De Gori R Walter M, Doughty L, Hattarki M, Hudson PJ, and Kortt AA. Single-chain Fv multimers of the anti-neuraminidase antibody NC10: the residue at position 15 in the V(L) domain of the scFv-0 (V(L)-V(H)) molecule is primarily responsible for formation of a tetramer-trimer equilibrium. Protein Eng. 2003;16(1):47–56. doi:10.1093/proeng/gzg006. PMID:12646692.
44. Whitlow M, Filpula D, Rollence ML, Feng SL, and Wood JF. Multivalent Fvs: characterization of single-chain Fv oligomers and preparation of a bispecific Fv. Protein Eng. 1994;7(8):1017–26. doi:10.1093/protein/7.8.1017. PMID:7809028.
45. Singh N, Perazzelli J, Grupp SA, and Barrett DM. Early memory phenotypes drive T cell proliferation in patients with pediatric malignancies. Sci Transl Med. 2016;8(320):320 ra3. doi:10.1126/scitranslmed.aad5222. PMID: 26738796.
46. Lathrop SK, Huddleston CA, Dullforce PA, Montfort MJ, Weinberg AD, and Parker DC. A signal through OX40 (CD134) allows anergic, autoreactive T cells to acquire effector cell functions. J Immunol. 2004;172(11):6735–43. doi:10.4049/jimmunol.172.11.6735. PMID:15153490.
47. Redmond WL, Gough MJ, Charbonneau B, Ratliff TL, and Weinberg AD. Defects in the acquisition of CD8 T cell effector function after priming with tumor or soluble antigen can be overcome by the addition of an OX40 agonist. J Immunol. 2007;179(11):7244–53. doi:10.4049/jimmunol.179.11.7244. PMID:18025166.
48. Liao W, Lin JX, and Leonard WJ. Interleukin-2 at the crossroads of effector responses, tolerance, and immunotherapy. Immunity. 2013;38 (1):13–25. doi:10.1016/j.immuni.2013.01.004. PMID:23352221.
49. Rossig C, Bollard CM, Nuchtern JG, Merchant DA, and Brenner MK. Targeting of G(D2)-positive tumor cells by human T lymphocytes engineered to express chimeric T-cell receptor genes. Int J Cancer. 2001;94(2):228–36. doi:10.1002/ijc.1457. PMID:11668503.
50. Pule MA, Straathof KC, Dotti G, Heslop HE, Rooney CM, and Brenner MK. A chimeric T cell antigen receptor that augments cytokine release and supports clonal expansion of primary human T cells. Molecular Therapy. 2005;12(5):933–41. doi:10.1016/j.ymthe.2005.04.016. PMID:15979412.
51. Yvon E, Del Vecchio M, Savoldo B, Hoyos V, Dutour A, Anichini A, Dotti G, and Brenner MK. Immunotherapy of Metastatic Melanoma Using Genetically Engineered GD2-Specific T cells. Clinical Cancer Research. 2009;15(18):5852–60. doi:10.1158/1078-0432.CCR-08-3163. PMID:19737958.
52. Di Stasi A, De Angelis B, Rooney CM, Zhang L, Mahendravada A, Foster AE, Heslop HE, Brenner MK, Dotti G, and Savoldo B. T lymphocytes coexpressing CCR4 and a chimeric antigen receptor targeting CD30 have improved homing and antitumor activity in a Hodgkin tumor model. Blood. 2009;113(25):6392–402. doi:10.1182/blood-2009-03-209650. PMID:19377047.
53. Singh H, Figliola MJ, Dawson MJ, Olivares S, Zhang L, Yang G, Maiti S, Manuri P, Senyukov V, Jena B, et al. Manufacture of clinical-grade CD19-specific T cells stably expressing chimeric antigen receptor using Sleeping Beauty system and artificial antigen presenting cells. PLoS One. 2013;8(5):e64138. doi:10.1371/journal.pone.0064138. PMID:23741305.
54. Savoldo B, Rooney CM, Di Stasi A, Abken H, Hombach A, Foster AE, Zhang L, Heslop HE, Brenner MK, and Dotti G. Epstein Barr virus specific cytotoxic T lymphocytes expressing the anti-CD30zeta artificial chimeric T-cell receptor for immunotherapy of Hodgkin disease. Blood. 2007;110(7):2620–30. doi:10.1182/blood-2006-11-059139. PMID:17507664.
55. Weber G, Caruana I, Rouce RH, Barrett AJ, Gerdemann U, Leen AM, Rabin KR, and Bollard CM. Generation of tumor antigen-specific T cell lines from pediatric patients with acute lymphoblastic leukemia–implications for immunotherapy. Clin Cancer Res. 2013;19(18):5079–91. doi:10.1158/1078-0432.CCR-13-0955. PMID:23838315.
56. Compagnucci C, Petrini S, Higuraschi N, Trivisano M, Specchio N, Hirose S, Bertini E, and Terracciano A. Characterizing PCDH19 in human induced pluripotent stem cells (iPSCs) and iPSC-derived developing neurons: emerging role of a protein involved in controlling polarity during neurogenesis. Oncotarget. 2015;6(29):26804–13. doi:10.18632/oncotarget.5757. PMID:26450854.
57. Cox J, and Mann M. MaxQuant enables high peptide identification rates, individualized p.p.b.-range mass accuracies and proteome-wide protein quantification. Nature biotechnology. 2008;26(12):1367–72. doi:10.1038/nbt.1511. PMID:19029910.
58. Vizcaino JA, Csordas A, Del-Toro N, Dianes JA, Griss J, Lavidas I, Mayer G, Perez-Riverol Y, Reisinger F, Ternent T, et al. 2016 update of the PRIDE database and its related tools. Nucleic acids research. 2016;44(D1):D447–56. doi:10.1093/nar/gkv1145. Epub 2015 Nov 2. PMID: 26527722.
59. Di Stasi A, De Angelis B, and Savoldo B. Gene therapy to improve migration of T cells to the tumor site. Methods Mol Biol. 2010;651:103–18. doi:10.1007/978-1-60761-786-0_7. PMID:20686963.
60. Hoyos V, Del Bufalo F, Yagyu S, Ando M, Dotti G, Suzuki M, Bouchier-Hayes L, Alemany R, and Brenner MK. Mesenchymal Stromal Cells for Linked Delivery of Oncolytic and Apoptotic Adenoviruses to Non-small-cell Lung Cancers. Mol Ther. 2015;23(9):1497–506. doi:10.1038/mt.2015.110. PMID:26084970.
61. Tyanova S, Temu T, Sinitcyn P, Carlson A, Hein MY, Geiger T, Mann M, and Cox J. The Perseus computational platform for comprehensive analysis of (prote)omics data. Nature methods. 2016;13(9):731–40. doi:10.1038/nmeth.3901. PMID:27348712.